Model of Intracellular Calcium Cycling in Ventricular Myocytes

Y. Shiferaw,* M. A. Watanabe,* A. Garfinkel,† J. N. Weiss,† and A. Karma*
*Department of Physics and Center for Interdisciplinary Research on Complex Systems, Northeastern University, Boston, Massachusetts 02115; and †Department of Medicine and Cardiology, University of California, Los Angeles, California 90095

ABSTRACT We present a mathematical model of calcium cycling that takes into account the spatially localized nature of release events that correspond to experimentally observed calcium sparks. This model naturally incorporates graded release by making the rate at which calcium sparks are recruited proportional to the whole cell L-type calcium current, with the total release of calcium from the sarcoplasmic reticulum (SR) being just the sum of local releases. The dynamics of calcium cycling is studied by pacing the model with a clamped action potential waveform. Experimentally observed calcium alternans are obtained at high pacing rates. The results show that the underlying mechanism for this phenomenon is a steep nonlinear dependence of the calcium released from the SR on the diastolic SR calcium concentration (SR load) and/or the diastolic calcium level in the cytosol, where the dependence on diastolic calcium is due to calcium-induced inactivation of the L-type calcium current. In addition, the results reveal that the calcium dynamics can become chaotic even though the voltage pacing is periodic. We reduce the equations of the model to a two-dimensional discrete map that relates the SR and cytosolic concentrations at one beat and the previous beat. From this map, we obtain a condition for the onset of calcium alternans in terms of the slopes of the release-versus-SR load and release-versus-diastolic-calcium curves. From an analysis of this map, we also obtain an understanding of the origin of chaotic dynamics.

INTRODUCTION

The contraction of a cardiac myocyte is triggered by an intracellular rise in calcium concentration that is due to a coordinated release of calcium from the sarcoplasmic reticulum (SR) (Fabiato, 1983). The release of calcium from the SR occurs via ryanodine receptors (RyR), which are in close proximity to L-type calcium channels that are located in the cell surface membrane and T-tubules (Meissner, 1994; Wang et al., 2001). When the cell is depolarized, L-type channels open and allow calcium entry into a confined microdomain. The rise of calcium in this small space is sensed by the nearby cluster of RyR channels that in turn open via calcium-induced calcium release (CICR) (Fabiato, 1983). As the calcium concentration in the cell rises, contractile elements are activated and the cell contracts. An uptake pump, which is activated by the rise in calcium, then pumps calcium back into the SR. This interplay between voltage across the cell membrane and intracellular calcium cycling forms the basis of excitation-contraction (EC) coupling.

During normal beating of the heart, myocardial cells undergo periodic depolarizations of the membrane called action potentials (AP). The shape of the AP waveform is determined by the flux of ions across the membrane. Some of these fluxes, such as those due to the L-type channel current (I_{Ca}) and the NaCa exchange current (I_{NaCa}), are modulated by intracellular calcium concentration. Thus, the calcium system is driven by an AP waveform that is itself dependent on the dynamics of the calcium system. Recently, Chudin et al. (1999) were able to shed light on this coupling by stimulating a rabbit ventricular myocyte using a clamped AP waveform. They observed that at high stimulation rates the whole cell calcium transients exhibited alternans even when the clamped voltage stimulus was periodic. This result demonstrates that the calcium system could be dynamically unstable independently of the dynamics of the membrane potential. Thus, given the bidirectional coupling between voltage and calcium, this raised the important possibility that abnormalities in calcium cycling could influence the membrane potential and hence promote arrhythmias. For example, ventricular fibrillation is typically preceded by ventricular tachycardia, where the ventricles can be driven at rapid rates by an unstable rotating spiral wave. It is possible that at high rates a dynamical instability of calcium cycling at the single cell level may promote wave break and thus underlie the transition of ventricular tachycardia to ventricular fibrillation. Therefore, a physiologically based model of calcium cycling is necessary to investigate this important bidirectional coupling of voltage and calcium. In particular, it is important that this model reproduces the experimentally observed complex dynamics of the calcium system at high stimulation rates.

There have been many efforts to model intracellular calcium dynamics. Initial modeling attempts were faced with the challenge of explaining the experimentally observed (Wier et al., 1994) linear dependence of calcium release from the SR on the whole cell I_{Ca} current (graded release), given that RyR channels are activated by a CICR mechanism that favors an all-or-none response. This issue was resolved by Stern (1992), who pointed out that graded release can be explained by the stochastic recruitment of independent local release fluxes. Stern referred to models of this type as local control models since a small cluster of L-type channels were coupled to a cluster of RyR channels via a local pool of calcium. Stern emphasized that models that couple whole

Submitted July 1, 2003, and accepted for publication September 9, 2003.

Address reprint requests to Alain Karma, Physics Dept., 110 Forsyth St., Northeastern University, Boston, MA 02115. Tel.: 671-373-2929; Fax: 671-373-2943; E-mail: a.karma@neu.edu.

0006-3495/03/12/3666/21 $2.00

cell I_{Ca} to RyR flux via a single pool, which he referred to as common-pool models, would not be able to explain graded release. This hypothesis was later confirmed by high resolution confocal imaging, which showed that the global rise in calcium was due to the summation of many local release events sometimes referred to as calcium sparks (Cannell et al., 1994; Cleemann et al., 1998; Lopez-Lopez et al., 1995; Niggli, 1999; Wier and Balke, 1999).

The local nature of the release has led researchers to explore the detailed calcium dynamics within the dyadic junction, i.e., the space between the L-type channel clusters and the corresponding RyR receptor clusters (Cannell and Soeller, 1997; Greenstein and Winslow, 2002; Rice et al., 1999; Peskoff and Langer, 1998; Sobie et al., 2002; Stern et al., 1999). However, it turns out to be difficult to characterize experimentally the gating kinetics of the RyR clusters and the interaction of these clusters with the L-type channels. As a result, these kinetics are still poorly understood and, in particular, the detailed mechanism by which release from the SR is terminated remains controversial (Bers, 2001; DelPrincipe et al., 1999; Niggli, 1999). Moreover, even if the calcium dynamics at the dyadic junction is precisely known, there are on the order of 10^4 junctions within a cell (Cleemann et al., 1998). Given that each junction is on a submicron scale, a modeling approach that attempts to resolve the dynamics of each junction is unlikely to be computationally tractable for modeling arrhythmogenesis at the tissue or organ level.

Several authors have proposed tractable phenomenological models of calcium cycling at the whole cell level (Chudin et al., 1999; Fox et al., 2002; Glukhovsky et al., 1998; Jafri et al., 1998; Luo and Rudy, 1994; Snyder et al., 2000; Viswanathan et al., 1999). However, several of these models (Jafri et al., 1998; Glukhovsky et al., 1998; Snyder et al., 2000) are common-pool models and, as Stern (1992) predicted, do not reproduce graded release. Hence, they do not correctly describe the coupling between the L-type calcium current and the release from the SR that is crucial to describe EC coupling. Viswanathan et al. (1999) presented an improved version of a model of release flux from the SR first presented in the Luo-Rudy II model (Luo and Rudy, 1994), which incorporates graded release. This model was able to reproduce calcium alternans in simulations performed in a ring of coupled cells, where the voltage waveform was not clamped (Hund et al., 2000). However, this model does not take into account the fact that the release from the SR is the summation of discrete release events. Consequently, it cannot, for example, describe the influence of the amplitude and duration of these events on the dynamics of calcium cycling and the instability mechanism responsible for alternans.

In this article, we present a new model of EC coupling in ventricular myocytes. This model distinguishes itself from previous models in that it represents release from the SR as a summation of elementary release events that correspond to calcium sparks. Furthermore, the model formulation is based on two experimentally measurable constitutive relations:

1. The relation between the rate of spark recruitment and the whole cell I_{Ca}. This relation describes quantitatively the crucial coupling between I_{Ca} and calcium release from the SR. This relation is formulated by introducing a variable, $N(t)$, which corresponds to the total number of sparks recruited at a given time t in the whole cell, and by making the rate of spark recruitment (dN/dt) proportional to the whole cell I_{Ca}. This linear relationship between dN/dt and I_{Ca} is based on the available experimental data on simultaneous measurements of spark occurrence and whole cell I_{Ca} (Collier et al., 1999; Lopez-Lopez et al., 1995) and reproduces graded release.
2. The relation between the total amount of calcium released form the SR and the SR load. This relation can be built into the model by letting the rate of spark recruitment and/or the average release current of a single spark depend on the junctional SR (JSR) concentration. This dependency is then chosen phenomenologically to reproduce the highly nonlinear relationship between fractional release and load that has been measured experimentally (Bassani et al., 1995).

Another important experimental input into the model is the observation (Cleemann et al., 1998; Niggli, 1999) that the lifetime of sparks is relatively constant and independent of both SR load and diastolic calcium level. Based on this observation, we model termination of release from the SR by assuming that the release current of a single spark decays exponentially in time from its initial peak value, with a time constant that is taken comparable to the observed spark lifetime.

The model includes additional features that are not present in previous models. The first is a phenomenological description of intracellular sodium accumulation. This accumulation is well documented experimentally (Harrison and Boyett, 1995), and was found necessary to reproduce the experimentally observed rise of diastolic calcium at high pacing rates. The second is the compartmentation of the myoplasm into a submembrane space near the sarcolemma and the rest of the myoplasm. This distinction recognizes the fact that the concentration in the submembrane space, which influences both the NaCa exchange current and the calcium-dependent inactivation of I_{Ca}, is much larger during release than the average bulk concentration inside the myoplasm, due to the proximity of this space to dyadic junctions. Finally, consistent with the discrete picture of sparking events, the model builds in a diffusional delay between the network SR and the JSR that distinguishes between the average JSR concentration of recruited and unrecruited dyadic junctions. We shall show here that this distinction leads to the interesting effect that this delay can enhance SR release, as opposed to always reducing it, as in previous models where the JSR is treated as a single pool (Jafri et al., 1998; Glukhovsky et al., 1998; Luo and Rudy, 1994).

We explore the dynamics of calcium cycling by pacing the model using a clamped AP waveform that is fitted to those

used in the experiments of Chudin et al. (1999). At high pacing rates, the model exhibits sustained calcium alternans, consistent with the experimental findings. Furthermore, we vary parameters of the model to identify which parts of the complex calcium cycling machinery are essential for alternans and which ones have a secondary role. We identify two essential instability mechanisms for alternans. The first is a steep relation between release and SR load, and the second is a steep relation between release and diastolic calcium that is due to calcium-induced inactivation of I_{Ca}. In addition, we find that the calcium dynamics can become chaotic even when paced with a periodic AP clamp.

To gain further insight into both alternans and chaotic dynamics, we reduce the ordinary differential equations (ODEs) of the model to a two-dimensional discrete map that relates the SR and cytosolic calcium concentrations at one beat to those at the previous beat. This map allows us to obtain a stability condition for the onset of calcium alternans with AP clamp pacing in terms of the slopes of the relations between release and SR load, and release and diastolic calcium, as well as the strength of the calcium uptake into the SR. In addition, this map allows us to show that the existence of chaos is due to a nonmonotonic relation between the peak calcium transient at one beat to that at the previous beat.

This article is organized as follows. In the next section, we describe the various intracellular compartments used in the model, and define the corresponding calcium concentrations. In the section ''SR Release Flux'', we describe a model for the SR release current. The calcium dependent membrane currents are then described in the section, ''Calcium Fluxes across the Sarcolemma''. In the section ''Dynamics of Calcium Cycling'', we integrate these currents into a set ODEs that are used to study calcium cycling. In the section ''Voltage Clamp Pacing'', we present the results of the model when paced under an AP clamp protocol. The reduction of this model to a map is then described in the section ''Analysis of Beat-to-Beat Dynamics'', and the results are used to analyze the dynamical behavior of the model. The results are discussed in the ''Discussion'' section, followed by ''Conclusions''.

INTRACELLULAR COMPARTMENTS AND CONCENTRATIONS

A schematic diagram of the intracellular compartments relevant to calcium cycling is given in Fig. 1. The SR is a spatially diffuse network of tubules and cisternae that is composed of two distinct parts. The first is the network SR (NSR), which is a meshwork of tubules that enwraps the myofilaments. These tubules branch out from the NSR into flattened elliptical sacs, referred to as the junctional SR, that position themselves close to the surface of the cell sarcolemma (Forbes et al., 1985; Franzini-Armstrong et al., 1999). The volume in between the JSR and the sarcolemma is the dyadic junction, wherein RyR channels in the JSR

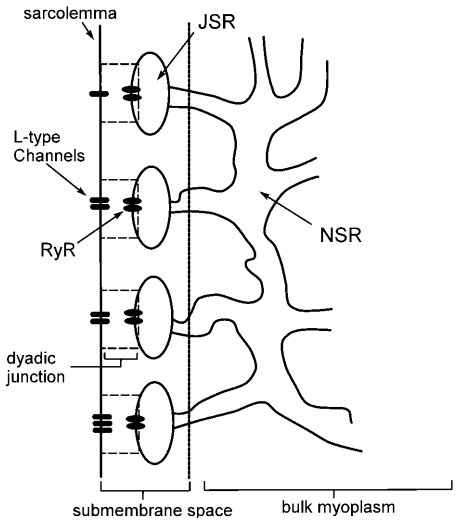

FIGURE 1 Illustration of the intracellular spaces.

membrane are in close proximity to L-type channels in the sarcolemma. In ventricular myocytes, the sarcolemma forms a uniform array of deep invaginations into the cell, referred to as T-tubules (Soeller and Cannell, 1999), which effectively distribute dyadic junctions uniformly throughout the cell.

The flux of calcium from the SR to the myoplasm, shortly after a voltage depolarization, is due to a summation of several thousand discrete local release events (Cannell et al., 1994; Cleemann et al., 1998). During the release process, calcium in the SR is being drained into the myoplasm via JSR compartments that are being depleted by local calcium release. To describe the calcium concentration within the SR during this release process, we first assume that the SR is composed of N_{jsr} identical JSR compartments, each with a volume, v_{jsr}, along with the bulk NSR with volume v_{nsr}. This gives a total SR volume of $v_{sr} = v_{nsr} + N_{jsr}v_{jsr}$. The total calcium concentration within the kth JSR compartment will be denoted by c_{jsr}^{k}, and the concentration in the NSR is c_{nsr}. At any given time, the JSR compartments can be divided into those that are being drained due to a spark in the local dyadic space, and those that are not. The average total calcium concentration within JSR compartments that are not being drained at time t will be denoted by $c_j'(t)$. This average is simply given by

$$c_j'(t) = \frac{1}{N_U(t)} \sum_{k \subset U} c_{jsr}^{k}(t), \tag{1}$$

where the summation is over the set of $N_U(t)$ unrecruited JSR compartments. The average total calcium concentration within the entire SR network, which includes all the JSR and the NSR, will be denoted by $c_j(t)$ and is given by

$$c_j(t) = \frac{1}{v_{sr}} \left[v_{nsr} c_{nsr}(t) + \sum_{k=1}^{N_{jsr}} v_{jsr} c_{jsr}^{k}(t) \right], \tag{2}$$

where the summation is over both recruited and unrecruited JSR volumes. It is important to distinguish between c_j and c_j', since in general $c_j \neq c_j'$. This is due to the finite time necessary for c_j' to relax to c_j via the diffusion of calcium ions within the SR network. During a local release, at the kth dyadic junction, for instance, c_{jsr}^k will drop below c_j as the JSR compartment is depleted. However, c_j' can be larger than c_j since the set of unrecruited JSR compartments are not depleted. This feature is quite different from previous models (Jafri et al., 1998; Glukhovsky et al., 1998; Luo and Rudy, 1994), where the entire JSR is treated as a single pool that is being replenished by the NSR. In such models, the JSR concentration is always less than the SR concentration during release.

To describe the calcium outside of the SR, we first divide this space into the bulk myoplasm (volume v_i, average free calcium concentration c_i), and a submembrane space (volume v_s, average free calcium concentration c_s), which corresponds to the space in between the bulk myoplasm and the sarcolemma (see Fig. 1). To clarify further, c_s is the average concentration that calcium-dependent membrane channels sense. Since membrane currents are delivered into v_s, and since $v_s \ll v_i$ (in this article we use $v_s/v_i \sim 10$), the concentration changes in the submembrane space are much larger and faster than those in the bulk myoplasm. This effect can potentially influence calcium-dependent ion channels at the sarcolemma. Also, the free calcium concentration within the kth dyadic junction will be denoted by c_p^k. It is important to note that the average volume of a dyadic space is $\sim 10^{-9}$ times smaller than that of the cell volume. Thus, during a calcium spark in the kth dyadic junction the concentration c_p^k can rise rapidly to levels >100 μM (Peskoff and Langer, 1998), whereas the concentration in the submembrane space will rise to ~5–10 μM.

SR RELEASE FLUX

Spark recruitment rate

To model the release process at the whole cell level, it is first necessary to determine the relationship between the number of release events (sparks) and the corresponding voltage stimulus. Since RyR channels are triggered by nearby L-type channels, it is reasonable to expect that spark recruitment is related to the total calcium current entering the cell via the L-type channels (I_{Ca}). Collier et al. (1999) have measured whole cell I_{Ca} simultaneously with calcium spark occurrence in rat ventricular myocytes, albeit under experimental conditions of reduced I_{Ca}, which allowed for the visualization of individual sparks. They showed that the time course (i.e., time constant of decreasing occurrence) of calcium sparks with sustained depolarization was statistically identical to the time course (i.e., the time constant of inactivation) of the I_{Ca} current. This confirmed the conclusions of an earlier study that was similar except that I_{Ca} was not measured (Lopez-Lopez, 1995). A more recent article (Sah et al., 2002) again shows in a quantitative manner that the time course of spark occurrence parallels the time course of I_{Ca}, using novel voltage clamp protocols, such as triangular and action potential waveforms.

To quantify the relationship between spark occurrence and the I_{Ca} current, we will denote the number of sparks recruited at time t to be $N(t)$. Then the rate of spark recruitment is $dN(t)/dt$, which is the number of sparks recruited in a whole cell per unit time. This rate can be computed directly from experimental measurements of spark occurrence. Using the experimental data presented in the work of Collier et al. (1999), we compared the rate of spark occurrence and the I_{Ca} current for a depolarization to a holding potential of 30 mV (see Fig. 4 in their article). In Fig. 2, we plot the computed spark rate as a function of whole cell I_{Ca}. It is clear from the plot that, under the physiological conditions of the measurement and for the given depolarization potential, the measured spark rate is to a good approximation proportional to whole cell I_{Ca}, i.e., $dN(t)/dt \propto I_{Ca}(t)$.

It is known experimentally that when the calcium content of the SR is increased, the frequency of spontaneous sparks in a resting myocyte also increases (Cheng et al., 1993; Lukyanenko et al., 1996, 2000). This dependence between spark occurrence and SR content implies that RyR channels are sensitive to the calcium concentration within the local JSR compartment. Now, since JSR compartments, which already have been depleted due to a spark, probably cannot be recruited until they have had enough time to refill, we expect that the rate of spark recruitment should depend on the average calcium concentration within unrecruited JSR compartments (c_j'). Thus, we model the JSR calcium dependence of the whole cell spark rate using

$$\frac{dN(t)}{dt} = gI_{Ca}(t)A(c_j'(t)), \tag{3}$$

where the function $A(c_j')$ gives the JSR load dependence, and where g is a proportionality constant.

Calcium release during a spark

The local release flux during a spark will be dictated by the gating kinetics of the RyR cluster and the calcium gradients

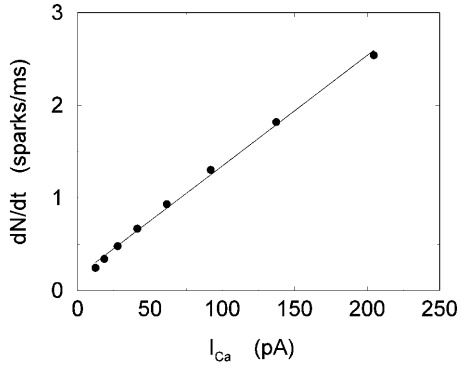

FIGURE 2 Spark rate versus whole cell I_{Ca} using the experimental data of Collier et al. (1999). The straight line corresponds to a linear fit.

in the dyadic space. However, because the detailed properties of a cluster of RyR channels are not well known, we will describe local release using a simple phenomenological model based on very general considerations. First, we will assume that a spark that is activated at a given time t', in the kth dyadic junction, is determined primarily by the local JSR concentration at the time of activation $c^{\mathrm{k}}_{\mathrm{jsr}}(t')$, rather than the concentration in the local dyadic space $c^{\mathrm{k}}_{\mathrm{p}}(t')$. This is a reasonable assumption because the free calcium concentration gradient across the RyR channels is extremely large, and once CICR is induced, the subsequent flux will rise to a value that is determined by the amount of releasable calcium in the JSR. We will also assume that once a spark is recruited it will have a constant lifetime denoted by $\tau^{\mathrm{k}}_{\mathrm{r}}$. This assumption is motivated by fluorescence measurements of calcium sparks (Cleemann et al., 1998; Niggli, 1999), which show that sparks have a well defined lifetime around 10–30 ms. Given these simplifying assumptions, the flux at time t, from the kth JSR compartment, during a spark that is activated at time $t' \leq t$, can be written as

$$I^{\mathrm{k}}_{\mathrm{spark}}(t,t') = J^{\mathrm{k}}(c^{\mathrm{k}}_{\mathrm{jsr}}(t'))e^{-(\mathrm{t}-\mathrm{t}')/\tau^{\mathrm{k}}_{\mathrm{r}}}, \tag{4}$$

where the function J^{k} gives the JSR load dependence of the local flux amplitude at the kth dyadic junction.

Once the whole cell I_{Ca} is activated, sparks are stochastically recruited at many dyadic junctions distributed throughout the cell. Thus, at a given time t', an ensemble of release fluxes given by Eq. 4 is recruited. Here, we will argue that this ensemble of spark fluxes has well-defined averaged properties. This averaging procedure will allow us to drop the superscript k in Eq. 4, and will simplify the subsequent analysis of spark summation. First, we note that $c^{\mathrm{k}}_{\mathrm{jsr}}(t')$ in Eq. 4 denotes the JSR concentration at the time t' when a spark is just being recruited. Thus, the kth JSR compartment has not yet been depleted and will have a concentration that is roughly the same as the average concentration in unrecruited JSR compartments $c'_{\mathrm{j}}(t')$. Hence, we can make the approximation that $c^{\mathrm{k}}_{\mathrm{jsr}}(t') \approx c'_{\mathrm{j}}(t')$. Second, we assume that the lifetime and amplitude of a spark in the kth dyadic junction is roughly the same as the average over the ensemble of recruited sparks. To be more precise, if we define the average $\tau_{\mathrm{r}} = \langle \tau^{\mathrm{k}}_{\mathrm{r}} \rangle$ and $J = \langle J^{\mathrm{k}} \rangle$, where the brackets denote an average over the ensemble of recruited sparks, then $\tau^{\mathrm{k}}_{\mathrm{r}} \approx \tau_{\mathrm{r}}$ and $J^{\mathrm{k}} \approx J$. This claim is equivalent to the statement that the distribution of spark lifetimes and amplitudes is narrowly peaked around their averages. This assumption is motivated by fluorescence images of calcium sparks that show that sparks in different regions of the cell essentially have the same spatial and temporal properties (Cleemann et al., 1998; Niggli, 1999). Thus, the local flux during a spark in the kth junction $I^{k}_{spark}(t, t')$, can be represented by an average spark flux $I_{\mathrm{spark}}(t, t')$, where $J^{\mathrm{k}} \rightarrow J$, $\tau^{\mathrm{k}}_{\mathrm{r}} \rightarrow \tau_{\mathrm{r}}$, and $c^{\mathrm{k}}_{\mathrm{jsr}}(t') \rightarrow c'_{\mathrm{j}}(t')$.

To asses the validity of Eq. 4, we have also developed a set of ODEs that describe the calcium dynamics within a dyadic junction. This model, given in detail in Appendix A, simulates a calcium spark using a simple CICR gating kinetics that is initiated by a short pulse of calcium injected into a simulated dyadic space. Local flux termination is then modeled using a combination of diffusion-driven deactivation and local JSR depletion. In Appendix A, we show that Eq. 4 approximates well the local current due to a simulated local release. However, it is important to note that Eq. 4 does not rely on any specific mechanism underlying the local calcium dynamics, and should hold under more general conditions. Thus, our simple model of the calcium dynamics at the dyadic junction level serves primarily to validate Eq. 4 in a particular case, but is not central to the overall implementation of the model.

Summation of calcium sparks

The total flux draining the SR at time t, which will be denoted by $I_{\mathrm{r}}(t)$, is given by the summation of local fluxes due to sparks recruited at times $t' \leq t$. To compute this sum, we divide the interval of time $0 \leq t' \leq t$ into M bins of duration $\Delta t'$, such that $t = M\Delta t'$. Consequently, the flux draining the SR at time $t = M\Delta t'$ is given by the discrete sum

$$I_{\mathrm{r}}(t) = \sum_{\mathrm{i}=1}^{\mathrm{M}} \Delta N(i\Delta t') I_{\mathrm{spark}}(t, i\Delta t'), \tag{5}$$

where $\Delta N(i\Delta t')$ is the number of sparks recruited during the time interval $(i-1)\Delta t' \leq t' \leq i\Delta t'$. If we now take the continuum limit $\Delta t' \rightarrow 0$ and use the expression for the average spark flux $I_{\mathrm{spark}}(t, t')$ (Eq. 4 where the superscript k is dropped), the above discrete sum becomes an integral

$$I_{\mathrm{r}}(t) = \int_0^{\mathrm{t}} \frac{dN(t')}{dt'} J(c'_{\mathrm{j}}(t')) e^{-(\mathrm{t}-\mathrm{t}')/\tau_{\mathrm{r}}} dt', \tag{6}$$

where $t' = 0$ is a time origin when $I_{\mathrm{r}}(0) = 0$. Finally, differentiating both sides of this equation with respect to t, we obtain

$$\frac{dI_{\mathrm{r}}(t)}{dt} = \frac{dN(t)}{dt} J(c'_{\mathrm{j}}(t)) - \frac{I_{\mathrm{r}}(t)}{\tau_{\mathrm{r}}}, \tag{7}$$

which will be our basic equation for the release flux $I_{\mathrm{r}}(t)$. Using Eq. 3, the first term on the right-hand side of Eq. 7 can be written as $(dN(t)/dt)J(c'_{\mathrm{j}}(t)) = gI_{\mathrm{Ca}}(t)A(c'_{\mathrm{j}}(t))J(c'_{\mathrm{j}}(t))$, which reveals that the JSR load dependence of release is governed by the function $Q(c'_{\mathrm{j}}) = A(c'_{\mathrm{j}})J(c'_{\mathrm{j}})$.

SR load dependence of release

The release of calcium as a function of SR load has been addressed experimentally (Bassani et al., 1995; Shannon et al., 2000b). In the experiment by Bassani et al. (1995), the fraction of SR calcium released as a function of SR load at

fixed trigger I_{Ca} was measured in ferret ventricular myocytes. The authors found that for low SR loads $[Ca]_{SRT} < 50$ μmol/l cytosol, almost no calcium is released. At normal loading $[Ca]_{SRT} \sim 90$ μmol/l cytosol, about half of the SR is released, whereas for slightly larger loading $[Ca]_{SRT} \sim 100$ μmol/l cytosol, almost 70% of the SR is released. Here, $[Ca]_{SRT}$ denotes the total calcium concentration in the SR, which is the quantity measured in the experiment. An important finding of this experiment is that the fraction of calcium released from the SR depends on the initial calcium concentration of the SR in a highly nonlinear fashion. To model this dependence of release on SR load, we will pick a functional form for $Q(c_j')$, which will reproduce the essential features of the experimental results. Since the dependence of release on load only enters through the function $Q(c_j')$, it is clear that this function itself should depend on c_j' in a nonlinear fashion. There can be several explanations for such a nonlinear dependence of local release on JSR load. One possible scenario is that by virtue of the gating kinetics of the local RyR channels, the amount of calcium released at a single dyad $J(c_j')$, may change nonlinearly with JSR load. Another independent possibility is that the sensitivity of the RyR channels may depend on c_j' in a nonlinear fashion. In this case, it would be the load dependence of the spark rate $A(c_j')$ that is a nonlinear function. However, the advantage of our phenomenological approach is that the function $Q(c_j')$ can be chosen by appealing directly to experimental data, without a complete model of the SR load dependence of release.

JSR-SR diffusional relaxation

To complete the model, we take into account the fact that the average total calcium concentration in the SR (c_j) is not the same as the average concentration of unrecruited JSR compartments (c_j'). This is due to the finite time necessary for calcium to equilibrate, via diffusion, over the entire volume of the SR. This effect can be incorporated into the model by letting c_j' relax to c_j using $dc_j'/dt = (c_j - c_j')/\tau_a$, where τ_a is a relaxation time. A rough estimate of τ_a, which has not yet been measured experimentally, is the average time for a calcium ion to diffuse from a local JSR compartment to the bulk NSR. If we take the effective diffusion coefficient of calcium ions in the SR to be $\sim$150 $(\mu m)^2/s$ (Stern et al., 1999), then the time for an unobstructed calcium ion to diffuse over a distance 1 μm, (which is roughly the average distance between the NSR and the sarcolemma) is $\sim$7 ms. However, the calcium ions are confined within the SR, which is a complex tubular network of diameter 25–50 nm (Forbes et al., 1985), and so the diffusion (translocation) time can actually be much longer. Thus, we will consider relaxation times within a fairly wide range of 1–100 ms, and discuss in detail the role of this time constant on the dynamical behavior of the calcium system.

CALCIUM FLUXES ACROSS THE SARCOLEMMA

L-type calcium current

In this model, we have approximated the rate of spark recruitment to be proportional to the whole cell I_{Ca} current entering the cell at that time. Hence, a correct formulation of whole cell I_{Ca} is an essential component of the model. The whole cell I_{Ca} current can be written as $I_{Ca} = MP_o i_{Ca}$, where M is the number of L-type channels in the cell, P_o is the time-dependent open probability of a single channel, and i_{Ca} is the single-channel current. We model the open probability of the L-type channel using $P_o = d_\infty fq$, where d_∞ is an instantaneous voltage dependent activation gate, f is a slow voltage dependent inactivation gate variable, and where q describes calcium-induced inactivation. It is important to note that L-type channels, within dyadic junctions where a spark has just been activated, will see a calcium concentration that is much larger than c_s. Thus, these channels will have a much lower open probability as compared to the open probability of channels in unrecruited dyadic junctions. Hence, at a given time t, calcium entry into the whole cell via $I_{Ca}(t)$ should be dominated by those L-type channels within unrecruited dyadic junctions. Since the average concentration sensed by these channels is roughly the same as c_s, then the calcium-dependent gate variable q should depend on c_s.

The kinetics of calcium inactivation is modeled using a simple first order scheme that yields

$$q_\infty = \frac{1}{1 + c_s/\tilde{c}_s}, \quad \tau_q = \frac{q_\infty}{k_o}. \tag{8}$$

The detailed parameters of the gate variables are given in Appendix B, and are chosen so that the time course of I_{Ca} is qualitatively similar to the most recent experimental measurements in rabbit myocytes (Puglisi et al., 1999).

To explore the role of calcium-induced inactivation on the overall dynamics of the system, it is essential to also investigate more general inactivation schemes. However, we found that simply generalizing Eq. 8 to higher order kinetics led to an I_{Ca} time course that was different from experimentally measured currents (Linz and Meyer, 1998; Puglisi et al., 1999). Following an approach similar to Fox et al. (2002), we modeled calcium-induced inactivation using a simple phenomenological scheme with

$$q_\infty = \frac{1}{1 + (c_s/\tilde{c}_s)^\gamma}, \tag{9}$$

and with τ_q a constant in the range 10–50 ms. With this model formulation the exponent γ can be varied, and a steeper c_s dependence of calcium-induced inactivation can be explored.

NaCa exchange current

The NaCa exchange current is taken directly from Luo-Rudy II (Eq. 31 in Appendix B). The exchange current is sensitive

to the intracellular sodium concentration (Na_i). Higher Na_i reduces the transmembrane sodium gradient and so reduces the efficiency of the NaCa exchange current at extruding calcium from the cell, which should lead to higher intracellular calcium. An investigation by Harrison and Boyett (1995) used guinea pig ventricular myocytes to study pacing rate dependent increases in twitch shortening. They showed that when the pacing rate was increased from 0.5 to 3 Hz, twitch shortening increased by 34%, whereas if sodium entry (I_{Na}) was blocked by tetrodotoxin, twitch shortening increased by only 8%. This result demonstrates that rate dependent changes in Na_i could have a substantial effect on intracellular calcium. Thus, we felt it imperative to include a phenomenological description of Na_i, where Na_i is taken to be an increasing function of the pacing rate.

Role of the submembrane space

As mentioned in ''Intracellular Compartments and Concentrations'', we have divided the myoplasm into two spaces: a submembrane space, which is the space in the vicinity of the sarcolemma, and the bulk myoplasm, which is the remainder of the cell volume. This compartmentation of the myoplasm is motivated by the recent experimental and modeling work of Weber et al. (2001). Here, it was shown in particular that the NaCa exchange current I_{NaCa}, due to its proximity to dyadic junctions, senses a calcium concentration that is different from the global cytosolic calcium concentration. Consequently, modeling studies showed that the time course of I_{NaCa} served as a much more efficient calcium efflux mechanism when it is coupled to the larger and faster concentration changes at the submembrane space (c_s) than when it was coupled to the bulk concentration (c_i). Likewise, by virtue of calcium-induced inactivation, the time course of I_{Ca} should depend on the calcium concentration in the vicinity of the sarcolemma. This effect is particularly important since the calcium released from RyR channels during calcium release is delivered into dyadic junctions that are close to the sarcolemma. Thus, L-type channels sense a much more rapid rise in calcium than that given by the rise of the global cytosolic calcium concentration. To model the effect of a submembrane space, we let the membrane currents I_{Ca} and I_{NaCa} flow into a compartment of volume $v_s \ll v_i$, before diffusing to the bulk myoplasm via a simple relaxational current $I_d = (c_s - c_i)/\tau_s$, with τ_s a relaxation time that we will take to be in the range 5–10 ms.

DYNAMICS OF CALCIUM CYCLING

In this section, we study calcium cycling by incorporating the various currents described in previous sections into a single model. Since our formulation of the SR release flux does not explicitly depend on the calcium concentration gradient between the JSR and the submembrane space, we are free to formulate the dynamics of the SR calcium concentration in terms of the total concentration in the SR, rather than the free calcium concentration. An advantage of using the total SR concentration is that it is the quantity that is measured directly in experiments (Shannon et al., 2000b). Calcium buffering in the cytosol will be taken into account by incorporating the buffering to troponin C, SR, and calmodulin sites, since these are the sites that bind the majority of calcium released from the SR (Shannon et al., 2000a). The buffering to SR and calmodulin sites are fast and will be treated as instantaneous, whereas the time dependent kinetics for the buffering to troponin C will be accounted for.

The equations for calcium cycling can be written as

$$\frac{dc_s}{dt} = \beta(c_s)\left[\frac{v_i}{v_s}\left(I_r(t) - \frac{(c_s - c_i)}{\tau_s} - I_{Ca}(c_s, V) + I_{NaCa}(c_s, V)\right) - I^s_{trpn}\right]$$

$$\frac{dc_i}{dt} = \beta(c_i)\left(\frac{(c_s - c_i)}{\tau_s} - I_{up}(c_i) - I^i_{trpn}\right)$$

$$\frac{dc_j}{dt} = -I_r(t) + I_{up}(c_i), \tag{10}$$

where the flux out of the SR satisfies

$$\frac{dI_r(t)}{dt} = gI_{Ca}(t)Q(c_j') - \frac{I_r(t)}{\tau_r}, \tag{11}$$

and where

$$\frac{dc_j'}{dt} = \frac{c_j - c_j'}{\tau_a}. \tag{12}$$

Here, I^s_{trpn} and I^i_{trpn} describe the time dependent buffering to troponin C in the submembrane and bulk myoplasm respectively. The functions $\beta(c_s)$ and $\beta(c_i)$ account for the instantaneous buffering to SR and calmodulin sites. The details of the buffering kinetics and parameters are given in Appendix C. Also, V denotes a time-dependent AP waveform.

The free concentration in the cytosol (c_i) and the submembrane space (c_s) are in units of μM, whereas the total concentration in the SR and the JSR is scaled by a constant factor v_{sr}/v_i, so that c_j is in units of μmol/l cytosol. All fluxes have been divided by the volume of the cytosol v_i, and have units of μM/s. Thus, currents can be converted to amperes by multiplying by the factor $2Fv_i$, where F is Faraday's constant. Also, the volume of the cytosol will be taken to be 10 times the volume of the submembrane space ($v_i/v_s = 10$). The parameters used in the model are given in Tables 1–4. It should be noted that the above equations do not mathematically forbid unphysiological draining of the SR, where c_j becomes less than zero. However, for physiologically plausible parameters, such as the ones used in our simulations, c_j is always positive.

TABLE 1 Physical constants and ionic concentrations

Parameter	Definition	Value
F	Faraday constant	9.65×10^4 C/mol
R	Universal gas constant	8.314J $mol^{-1}K^{-1}$
T	Temperature	308 K
Na_o	External sodium concentration	140 mM
Ca_o	External calcium concentration	1.8 mM
v_i	Cell volume	10^{-4} μl
v_s	Submembrane volume	0.1 v_i

The constant g will be taken to have units of sparks/μM, so that gI_{Ca} gives the rate, in units of sparks/s, that sparks are recruited in the whole cell. The release function $Q(c_j')$ is taken to have the simple form

$$Q(c_j') = \begin{cases} 0 & 0 < c_j' < 50\,\mu\text{M} \\ c_j' - 50 & 50\,\mu\text{M} \le c_j' < 115\,\mu\text{M}, \\ uc_j' + s & c_j' \ge 115\,\mu\text{M}, \end{cases} \tag{13}$$

where u is an adjustable constant, and where s is fixed by the condition that the release function is continuous. Here, the flux $Q(c_j')$ is expressed in units of 10^{-3} μM/s, which, for a typical JSR load of $c_j' = 100$ μM, yields a local release current of ~1 pA, which is roughly the same as the experimental estimate of local release flux (Cheng et al., 1993). With the above choice of units we will use $g = 1.5 \times 10^4$ sparks/μM. Thus, for a total calcium entry, during a 1-s cycle, of $\int I_{Ca}\,dt \sim 2.5\,\mu$M, $\sim 4 \times 10^4$ sparks are recruited.

The constant u is adjusted so that the fractional release is consistent with the experimental results of Bassani et al. (1995). The fractional release is defined as

$$f(c_j^0) = \frac{c_j^0 - c_j^{\min}}{c_j^0}, \tag{14}$$

where c_j^0 is the total SR concentration just before an AP upstroke, and where $c_j^{\min}$ is the minimum total SR concentration shortly after the upstroke. To compute the fractional release, we clamp the voltage from $V_{\min} = -80$ mV to $V_{\max} = 30$ mV. Under these conditions, I_{Ca} quickly peaks and decays during which the SR concentration crosses a minimum value. By computing the minimum value $c_j^{\min}$ for various initial SR loads, we can compute the function $f(c_j^0)$. In Fig. 3 *A* we plot the fractional release f versus the initial SR load c_j^0 for the parameters given in Tables 1–4.

An important experimental observation that has to be incorporated into any model of EC coupling is graded release. In an important experiment, Wier et al. (1994) measured peak SR flux and peak I_{Ca} during depolarizations to various test potentials. In a similar manner, we held the membrane voltage at a $V(t)$ of -80 mV, and depolarized to various test potentials (V_{max}). As expected, and similar to Wier's results, peak I_{Ca} and peak I_r were bell shaped as a function of V_{max} (Fig. 3 *B*), and peak SR flux was graded with respect to peak I_{Ca}. The parameters were adjusted to give a gain (I_r^{max}/I_{Ca}^{max}) of ~10 for V_{max} in the range 0–30 mV (Wier et al., 1994).

TABLE 3 Exchanger and uptake parameters

Parameter	Definition	Value
c_{up}	Uptake threshold	0.5 μM
v_{up}	Uptake strength	250 μM/s
$\bar{I}_{NaCa}$	Adjustable strength of exchanger	2×10^4 μM/s
k_{sat}	Luo-Rudy II constant	0.1
ξ	Luo-Rudy II constant	0.35
$K_{m,Na}$	Luo-Rudy II constant	87.5 mM
$K_{m,Ca}$	Luo-Rudy II constant	1.38 mM

VOLTAGE CLAMP PACING

Pacing protocol

In the experiment of Chudin et al. (1999), intracellular calcium transients were measured as the cell was paced with various AP clamps. The AP clamp used in that experiment can be modeled effectively using

$$V(t) = \begin{cases} V_{\min} + (V_{\max} - V_{\min})\sqrt{1 - \left(\dfrac{t - mT}{xT}\right)^2} & mT \le t \le mT + xT \\ V_{\min} & mT + xT < t < (m+1)T, \end{cases} \tag{15}$$

TABLE 2 L-type channel parameters

Parameter	Definition	Value
P_{Ca}	Constant defined in Luo-Rudy II model	5.4×10^{-4} cm/s
$\bar{i}_{Ca}$	Adjustable proportionality constant	25 μmol C^{-1} cm^{-1}
τ_f	Voltage dependent inactivation gate constant	30 ms
k_o	Transition rate to open state	8 s^{-1}
$\tilde{c}_s$	Calcium inactivation threshold	0.5 μM

TABLE 4 SR release parameters

Parameter	Definition	Value
g	Release current strength	1.5×10^4 sparks/μM
u	Release slope	11.3 s^{-1}
τ_r	Spark lifetime	20 ms
τ_a	Relaxation time of c_j' to c_j	50 ms
τ_s	Submembrane diffusion time constant	10 ms

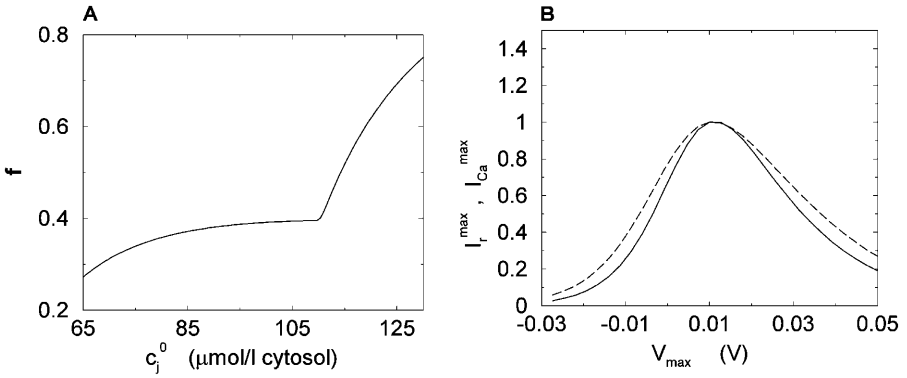

FIGURE 3 (*A*) Fractional SR release f versus initial SR load c_j^0. For all points, the initial conditions are $c_s(0) = c_i(0) = 0.1$ μM, $f(0) = 1$, $d(0) = 0$, $q(0) = 0.8$, $I_r(0) = 0$ μM/s. (*B*) Relationship between peak I_{Ca} and peak SR flux. The solid line is $I_r^{max}(V_{max})$, and the dashed line is $I_{Ca}^{max}(V_{max})$. Both curves have been normalized to their peak values. The initial conditions are identical to those given above except that the initial total SR load is fixed at $c_j(0) = 100$ μmol/l cytosol.

where T is the period (pacing cycle length), $x = APD/T$, where APD denotes the action potential duration, and where m denotes the mth beat. The parameter x fixes the shape of the AP, and depends on the pacing period. The action potentials are fitted using $V_{min} = -80$ mV and $V_{max} = 30$ mV. The ratio $x = APD/T$ was fitted to the experimental values using a function of the form

$$x(T) = \frac{a}{a + T}. \tag{16}$$

In Fig. 4 *A*, we plot the experimental values for x as a function of T, as well as the values given by a fit with $a = 2/3$.

Intracellular sodium and the rise of the calcium transients

The average whole cell sodium concentration Na_i depends on the amount of sodium injected into the cell during pacing, and so depends on the pacing period T. Since our model does not describe intracellular sodium dynamics, we introduce a function $Na_i(T)$, which gives the internal sodium concentration at steady state as a function of period T. Faber and Rudy (2000) have suggested that Na_i increases from ~10 mM to close to 15 mM, as the pacing period is decreased from 2 s to 100 ms. Hence, we model the intracellular sodium concentration using a simple function of the form

$$Na_i(T) = \frac{a}{1 + bT^{1/2}}, \tag{17}$$

where the constants a, b are chosen so that $Na_i(1\ s) = 9.6$ mM and $Na_i(.2\ s) = 18.5$ mM. In Fig. 4 *B*, we plot c_i^{max} and c_i^{min} after steady state has been reached for the above set of parameters. On the same graph we include the experimental data of Chudin et al. (1999). As we can see, both quantities rise with decreasing period, as $c_i^{max} - c_i^{min}$ remains fairly constant. On the same graph we plot the same quantities when intracellular sodium concentration is kept constant at $Na_i = 10$ mM. In this case there is only a small rise in c_i^{max}. Hence, in this model, the overall rise in calcium concentration during rapid pacing is primarily due to the accumulation of sodium in the cell.

Calcium transients and currents during rapid pacing

We studied the effects of pacing rate by pacing the calcium system with the clamped AP waveform at different cycle lengths (T). Results of pacing the model at a slow rate, with pacing cycle length of $T = 1$ s, and a fast rate, with cycle length $T = 0.25$ s, are shown in Figs. 5 and 6, respectively. Both sets of figures show the steady state values of c_i, whole cell I_{Ca}, and the NaCa exchange current I_{NaCa}. The results of Fig. 6 show clearly that as the whole cell calcium transient alternates, so do the calcium-dependent currents. We explored the dynamics of the model more fully by calculating the peak calcium transient values at different pacing periods (Fig. 7). On the same graph, we plot the experimental data of Chudin et al. (1999). It is clear from the graph that as the period is decreased, the calcium system undergoes a period-doubling bifurcation, qualitatively similar to the experimental findings.

ANALYSIS OF BEAT-TO-BEAT DYNAMICS

Map reduction with linear instantaneous buffering

To understand the nonlinear dynamics of the calcium system, it is useful to reduce the dynamics of the model ODEs to a system of discrete maps. Using this approach, it is possible to understand the dynamical instability that is responsible for calcium alternans. To make the analysis more tractable, we first focus on the simple case where all cytosolic calcium buffering is linear and instantaneous; in this case, $\beta(c_s) = \beta_s$, and $\beta(c_i) = \beta_i$, where β_i and β_s are constants. This simplification is introduced mainly because it allows us to derive a simple analytical condition for the onset of calcium alternans, which makes transparent the physiological mechanisms that underlie this phenomenon. In the section ''Map reduction with instantaneous nonlinear buffering'', we then show that a more elaborate map derived with instantaneous, albeit nonlinear, buffering can yield predictions of calcium dynamics that are in reasonable quantitative agreement with the full model ODEs.

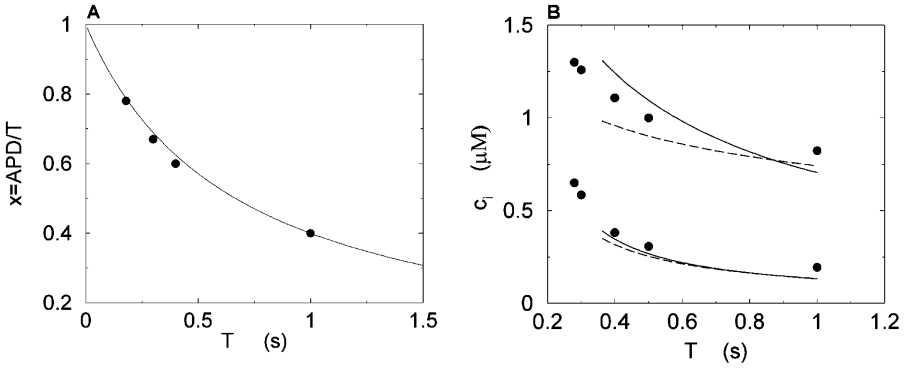

FIGURE 4 (*A*) Plot of the ratio $x = APD/T$ versus T. The circles correspond to values of x computed from the experimental AP clamps, and the line is the corresponding fit. (*B*) Maximum and minimum of bulk myoplasmic calcium concentration during steady state as a function of pacing period T at relatively slow pacing rates. The solid lines are for the case when the internal sodium concentration increases with decreasing period according to Eq. 17. The filled circles correspond to the experimental data points from Chudin et al. (1999). The dashed line corresponds to the case when intracellular sodium is fixed at $Na_i = 10$ mM.

Recall that our basic model (Eqs. 10–12) consists of four variables that represent the average concentrations in the cytosol, $c_i(t)$; the submembrane space, $c_s(t)$; the JSR, $c'_j(t)$; and the SR, $c_j(t)$. Furthermore, let us define $c_i^n \equiv c_i(nT)$, $c_s^n \equiv c_s(nT)$, $c_j^n \equiv c_j(nT)$, and $c'^n_j \equiv c'_j(nT)$, to be these concentrations at a time $t = nT$ just before the nth AP upstroke. The abruptness of the AP upstroke makes this a natural choice of variables for the discrete map. A mapping between these concentrations at the nth and nth + 1 AP upstrokes can be constructed by integrating the model ODEs from time $t = nT$ to time $t = (n + 1)T$. A major simplification is that the concentrations in the cytosol and the submembrane space are to a very good approximation equal before an AP upstroke ($c_s^n \approx c_i^n$) and only differ significantly from each other during the upstroke of the calcium transient. This is due to the fact that the volume of the submembrane space is much smaller than the volume of the cytosol ($v_i/v_s \gg 1$), and hence c_s relaxes quickly to c_i. Hence, the two concentrations are essentially equal except when c_i is rapidly varying. Similarly, the concentrations in the SR and in the JSR can be assumed to be equal just before an AP upstroke ($c_j^n \approx c'^n_j$) as long as the time for calcium to diffuse between these two compartments ($\tau_a \sim 50$ ms) is much smaller than the pacing interval ($\tau_a \ll T$). Using the fact that both $c_s^n \approx c_i^n$ and $c_j^n \approx c'^n_j$, it is straightforward to obtain from Eq. 10 the map

$$c_i^{n+1} = c_i^n + \alpha[R(c_i^n, c_j^n; T) - U(c_i^n, c_j^n; T) + \Delta(c_i^n, c_j^n; T)], \quad (18)$$

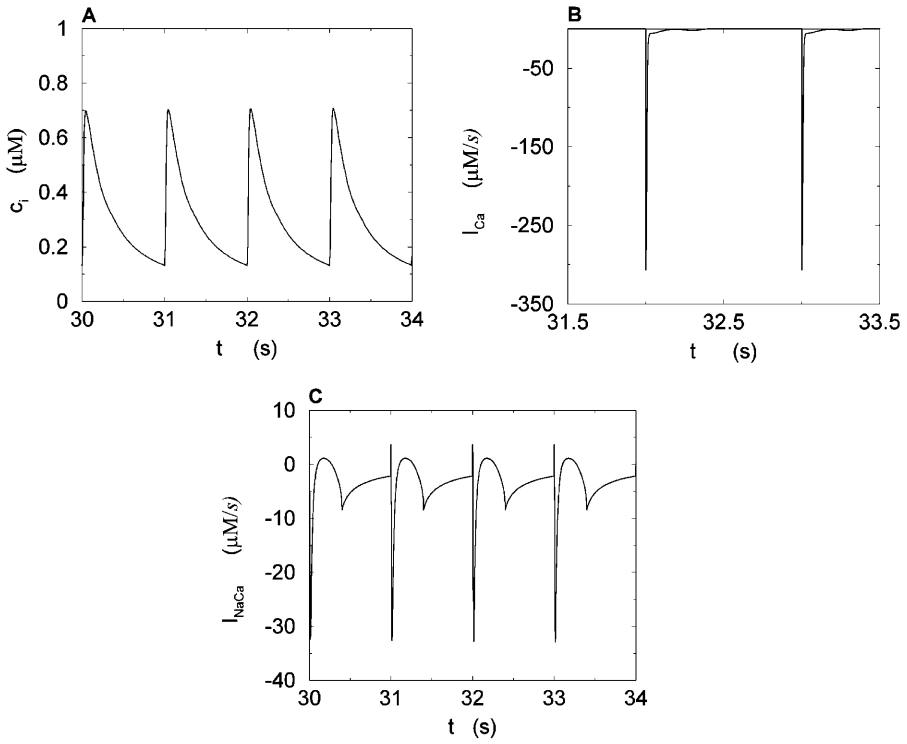

FIGURE 5 Calcium transients and currents during steady state for a pacing period of $T = 1$ s. (*A*) Plot of c_i versus t. (*B*) Plot of I_{Ca} versus t. (*C*) Plot of I_{NaCa} versus t.

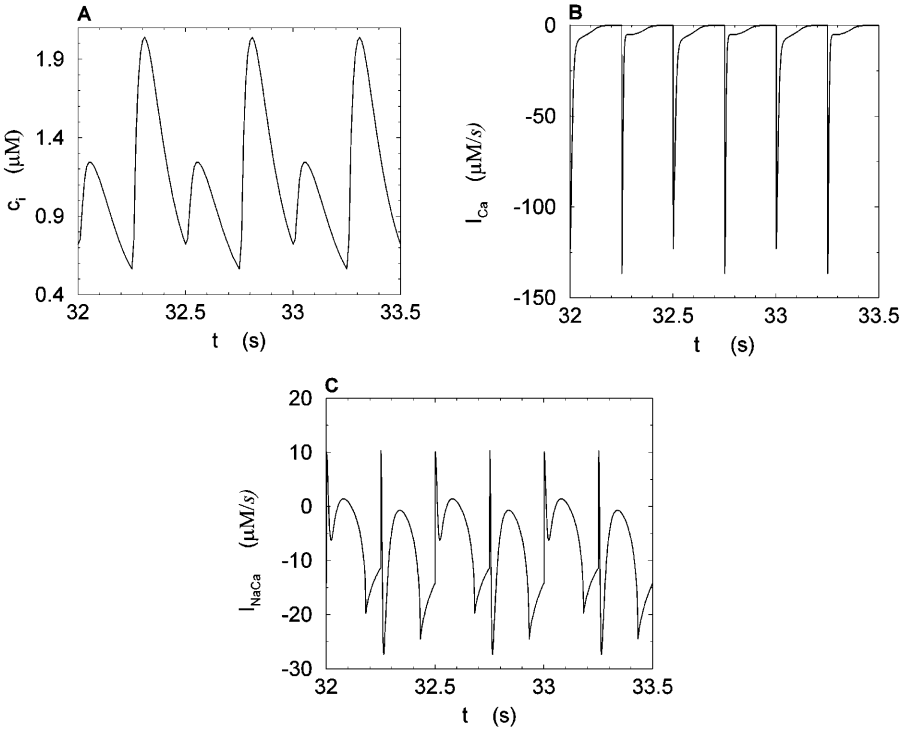

FIGURE 6 Calcium transients and currents during steady state for a pacing period of $T = 0.250$ s. (*A*) Plot of c_i versus t. (*B*) Plot of I_{Ca} versus t. (*C*) Plot of I_{NaCa} versus t.

$$c_j^{n+1} = c_j^n + [-R(c_i^n, c_j^n; T) + U(c_i^n, c_j^n; T)], \qquad (19)$$

where $\alpha = \beta_i/(1 + \beta_i \upsilon_s/\beta_s \upsilon_i)$, and where we have defined the quantities

$$R(c_i^n, c_j^n; T) = \int_{nT}^{(n+1)T} I_r(t)dt,$$

$$U(c_i^n, c_j^n; T) = \int_{nT}^{(n+1)T} I_{up}(t)dt,$$

$$\Delta(c_i^n, c_j^n; T) = \int_{nT}^{(n+1)T} [-I_{Ca}(t) + I_{NaCa}(t)]\, dt, \qquad (20)$$

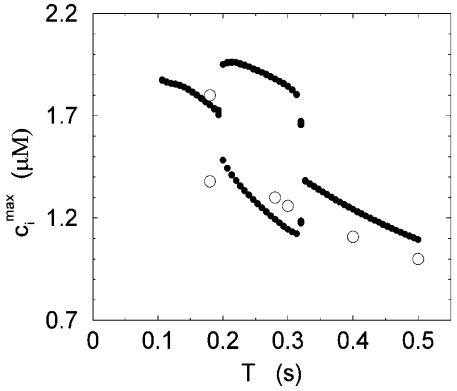

FIGURE 7 Peak values of the bulk myoplasmic calcium concentration during steady state as a function of pacing period T at fast pacing rates. The open circles correspond to the experimental results of Chudin et al. (1999). The filled circles correspond to the model predictions.

which represent the total amount of calcium release (R) and uptake (U) in one beat as well as the net total amount of calcium (Δ) that enters the cell. Both R and U are always positive whereas Δ can be either positive or negative depending on whether the amount of calcium that enters the cell through the L-type channels is larger or smaller than the amount of calcium extruded from the cell by the NaCa exchange current in one beat. The currents that appear in the integrals above must be calculated by integrating the full set of ODEs (Eqs. 10–12) for the variables ($c_s(t)$, $c_i(t)$, $c_j(t)$, and $c_j'(t)$) using as initial conditions $c_s(nT) = c_i(nT) = c_i^n$ and $c_j(nT) = c_j'(nT) = c_j^n$, and values of the gate variables $d_\infty(nT)$ and $f_\infty(nT)$ for I_{Ca} that are determined by the periodic clamped AP waveform.

Calcium alternans

In the rest of this section, we further analyze this map to pinpoint the condition for the onset of alternans. The fixed point of the map $c_i^n = c_i^0$ and $c_j^n = c_j^0$ is defined by the conditions $R = U$ and $\Delta = 0$, which implies that at steady state the total uptake during one cycle should be equal to the total release, and the net total flux into the cell over one period should be zero.

To obtain a simple analytical condition for the onset of alternans, we assume that the beat-to-beat variation of the net free calcium that enters the cell in one beat is much smaller than the variation of the total amount of calcium pumped into the SR ($|\Delta| \ll U$). This limit is physiologically relevant since the total calcium uptake in one beat is typically 3–4

times larger than the amount of calcium extruded from the cell via the NaCa exchange current (except in diseased states such as heart failure where the uptake and extruded amounts can become comparable). In this limit, the total diastolic amount of calcium in the cell (i.e., including both the myoplasm and the SR) can be assumed to remain approximately constant from beat to beat, or

$$c_i^n/\alpha + c_j^n \approx c_i^0/\alpha + c_j^0. \quad (21)$$

The above relation allows us to reduce the system of two coupled maps Eqs. 18 and 19 to a single map. One last simplification comes from our numerical finding that the amount of calcium uptake is roughly proportional to the peak concentration of the calcium transient, which is the sum of the diastolic value of c_i and the total amount released from the SR, or $c_{peak}^n \equiv c_i^n + \alpha R(c_i^n, c_j^n)$. This proportionality relation can be written

$$\alpha U(c_i^n, c_j^n) \approx w(T)c_{peak}^n = w(T)[c_i^n + \alpha R(c_i^n, c_j^n)], \quad (22)$$

where the proportionality constant $w(T)$ is cycle length dependent and always less than unity owing to the fact that the amount of calcium uptake cannot exceed the peak calcium concentration. Combining the above, we obtain the one-dimensional map defined by Eq. 19 with U approximated using Eq. 22 and c_i^n eliminated in favor of c_j^n using Eq. 21. A condition for the onset of alternans can now be readily obtained by substituting $c_j^n = c_j^0 + \delta c_j^n$ into the map, where δc_j^n is a small perturbation around the periodic fixed point. Linearizing the map one obtains $\delta c_j^{n+1} = -\Gamma \delta c_j^n$, where

$$\Gamma = (1 - w(T))\left(-1 - \alpha\frac{\partial R}{\partial c_i^n} + \frac{\partial R}{\partial c_j^n}\right), \quad (23)$$

and where the partial derivatives are evaluated at the fixed point. This fixed point undergoes a period doubling bifurcation when $\Gamma = 1$, and is unstable when $\Gamma > 1$.

The above analysis shows that calcium alternans under a clamped periodic AP waveform can arise from a sufficiently steep nonlinear dependence of calcium-release R on both SR load (c_j^n) and diastolic calcium level (c_i^n), with the latter influencing the trigger for release via calcium-induced inactivation of the L-type calcium current. These concentration-dependent restitution properties of the calcium system have a similar destabilizing role as APD-restitution (i.e., dependence of APD on diastolic interval) has for electrical alternans. In particular, the condition $\Gamma > 1$ for the onset of calcium alternans is directly analogous to the condition APD-restitution-slope > 1 for the onset of electrical alternans (Nolasco and Dahlen, 1968). Of course, predicting the onset of either calcium or electrical alternans in the more complex case where the AP is unclamped requires a careful consideration of the bidirectional coupling between the voltage and calcium systems.

To test the predictions of the stability condition given by Eq. 23 against the full model equations, we study how the onset of alternans depends on various model parameters. The condition for the onset of alternans, given by Eq. 23, predicts that at a given cycle length, an increase in the slope of the SR load dependence of release should promote alternans. In Fig. 8 *A*, we plot c_i^{max} versus T for various values of the release slope u. Recall that u is the slope of the steep part of the release function given in Eq. 13. From the graph, it is clear that the onset of the period doubling bifurcation is sensitive to the release slope u. As u is increased, the period-doubling bifurcation occurs at higher values of T, and the degree of alternans become more pronounced.

A further prediction of Eq. 23 is that the onset of alternans should also depend on the functional relationship between the release and the diastolic calcium level c_i^n. This functional dependence is primarily due to the calcium-induced inactivation of the L-type calcium channel, i.e., larger diastolic calcium should yield less release. Thus, by varying the steepness of calcium-induced inactivation, which is controlled by the parameter γ, it is possible to probe the effect on dynamics of a steeper c_i^n dependence of release. In Fig. 8 *B*, we plot c_i^{max} versus T for different exponents γ, while keeping the load dependence of release fixed. From the graph, it is clear that the period of onset and the magnitude of alternans increases with increasing γ. This shows clearly that the dynamical behavior of the model depends crucially on the calcium-induced inactivation of the L-type current.

The stability condition given by Eq. 23 also reveals that the onset of alternans depends on the strength of the uptake current. The prediction is that a larger uptake current (i.e., larger $w(T)$) should actually stabilize the periodic fixed point, since Γ decreases with increasing $w(T)$. To check this prediction in the model, in Fig. 8 *C* we plot the bifurcation diagram for different values of the strength of the uptake current (υ_{up}). From the plot, we see that decreasing the strength of the uptake current increases the period at which alternans occurs, which is consistent with the predictions of the stability analysis.

Finally, in Fig. 8 *D*, we plot the bifurcation diagram for the case when the release slope (u) is very large. Here, we find that the calcium system can undergo a transition to more complex dynamical behavior as the period is decreased. In this particular case, we observe a transition from a period 2 to a period 4, and then a subsequent transition to chaotic (aperiodic) dynamics.

Map reduction with instantaneous nonlinear buffering

Here, we only make the approximation that buffering to troponin C is instantaneous. This approximation is valid since the binding kinetics of troponin C to calcium ions occurs on a time scale of ~30 ms, which is fast compared to the movement of calcium ions in the cytosol. Thus, buffering

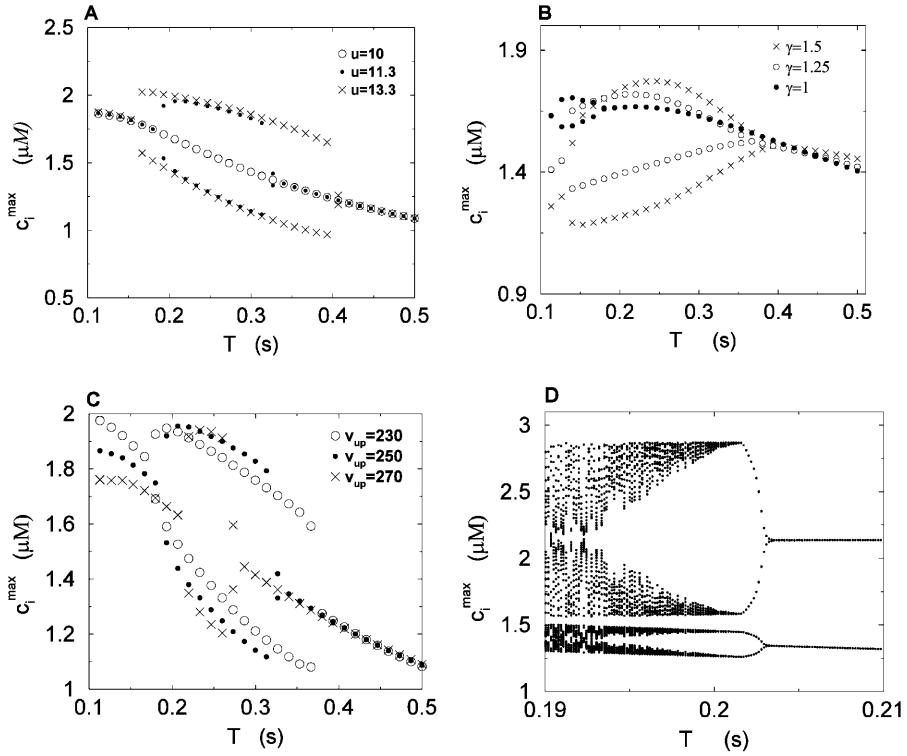

FIGURE 8 Peak values of bulk myoplasmic calcium concentration during steady state pacing as predicted by the model ODEs. (*A*) Peak calcium concentrations for different values of the release slope u. In all cases we fix $\gamma = 1$. (*B*) Peak calcium concentrations for different values of the parameter γ. In all cases the release slope is fixed at $u = 11.3\ s^{-1}$, and $\tau_q = 30$ ms. (*C*) Peak calcium concentrations for different values of the strength of the uptake current v_{up}. Here, we fix $\gamma = 1$ and $u = 11.3\ s^{-1}$. (*D*) Peak calcium concentrations for large release slope ($u = 43.3\ s^{-1}$).

to troponin C can be accounted for by simply adding a term $B_T K_T/(c_i + K_T)^2$, with $K_T = k_{off}^T/k_{on}^T$, inside the square brackets of Eq. 34 in Appendix C. In this way the time-dependent kinetics of calcium binding to troponin C can be eliminated from Eqs. 10. Applying the approximations discussed in the section ''Map reduction with linear instantaneous buffering'', ($c_s(nT) \approx c_i^n$, $c_j'(nT) \approx c_j^n$, $f(nT) \approx f_\infty(V(nT))$, $q(nT) \approx q_\infty(c_i^n)$)), all dynamical variables at times $t = nT$ can be uniquely defined by the concentrations c_i^n and c_j^n. Thus, integrating the model ODEs from $t = nT$ to $t = (n + 1)T$ defines a unique two-variable mapping $\{c_i^n, c_j^n\} \rightarrow \{c_i^{n+1}, c_j^{n+1}\}$.

In Fig. 9, we compare the steady-state peak calcium concentration (c_i^{max}) versus pacing cycle length (T) obtained with the map and the full model ODEs. The map predicts reasonably well the amplitude of alternans and their existence over a finite range of cycle lengths. It should be noted that the quantitative discrepancy between the map and ODE results is more pronounced for short cycle lengths. This is because the map derivation is based on the assumption that there is sufficient time for the dynamical variables of the ODEs to relax to values that are defined by c_i^n, c_j^n, and $f_\infty(V(nT))$, just before an AP upstroke. This assumption loses progressively its validity as the pacing cycle decreases. For instance, we assumed that $c_j'(nT) \approx c_j^n$. However, in the model ODEs, the time constant of the exponential relaxation of $c_j'(t)$ to c_j^n is 50 ms. Thus, for cycle lengths in the range of 100–200 ms, $c_j'(t)$ lacks sufficient time to fully relax to c_j^n before the next AP upstroke.

Chaotic dynamics

In this section, we analyze in more detail the chaotic dynamics observed in Fig. 8 *D*. For this, we first plot in Fig. 10*A* c_j^{n+1} versus c_j^n for the same parameters as in Fig. 8 *D* and for a pacing cycle length where chaotic dynamics is observed ($T = 0.19$ s). The plot shows that the chaotic attractor can be characterized to a good approximation by a one-dimensional map of c_j^{n+1} as a function of c_j^n. The one-dimensional character of this map is due to the fact that the net calcium entry into the cell via I_{Ca} and I_{NaCa} is small in comparison to

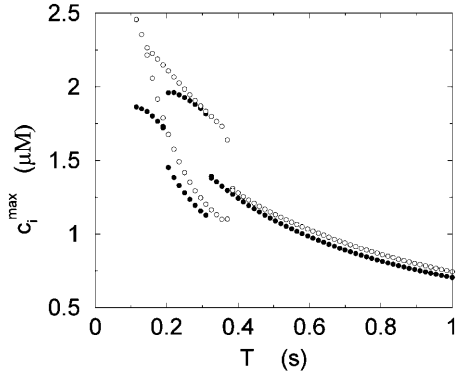

FIGURE 9 Peak values of the bulk myoplasmic calcium concentration during steady-state pacing. The filled circles correspond to values predicted by the model ODEs. The open circles are found using the two-dimensional map described in the section ''Map reduction with instantaneous nonlinear buffering''.

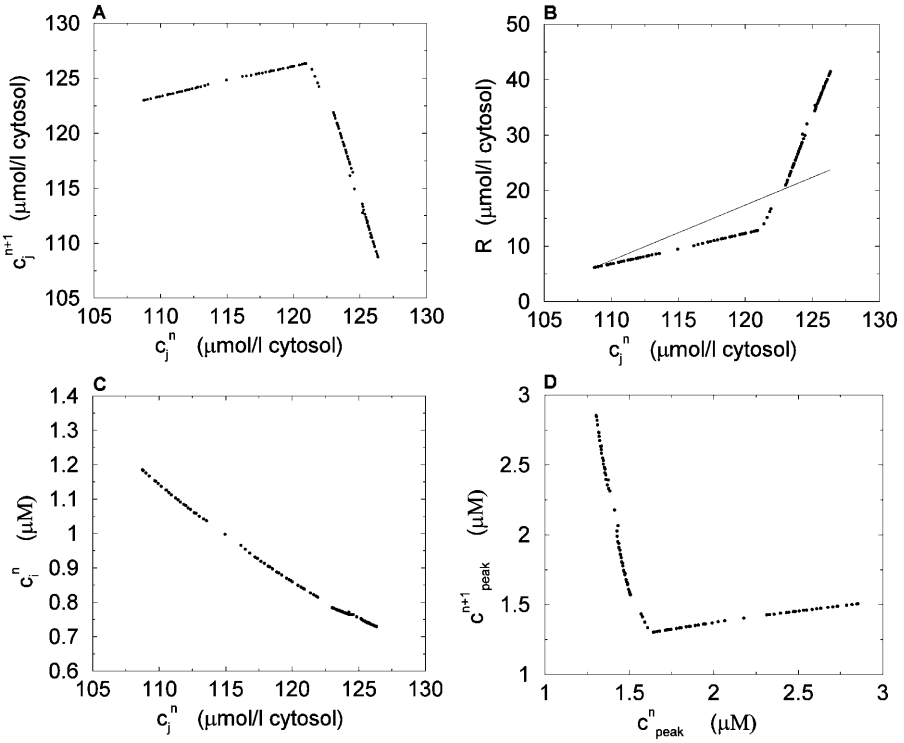

FIGURE 10 Plot of the beat-to-beat calcium concentrations during a chaotic calcium transient that is generated using the model ODEs. The parameters are the same as those used in Fig. 8 *D* with $T = 0.19$ s. (*A*) Plot of c_j^{n+1} versus c_j^n. (*B*) Plot of the release R versus initial SR load c_j^n. The straight line corresponds to a line with slope 1. (*C*) Plot of c_i^n versus c_j^n. (*D*) Plot of peak calcium transients c_{peak}^{n+1} versus c_{peak}^n.

the total amount of calcium that cycles through the SR in one beat. Therefore, as in our previous analysis of the stability of alternans, we can assume that the total calcium level inside the cell remains constant. Hence, we can use Eq. 21, $c_i^n/\alpha + c_j^n = c_{total}$, where c_{total} is the constant total concentration in the cell, to reduce the two-dimensional map to a one-dimensional map. Substituting this relation into Eq. 19 and making use of Eq. 22 to approximate the uptake with a constant factor w that only depends on period, we find that the diastolic SR load c_j^n satisfies the one-dimensional map $c_j^{n+1} = F(c_j^n)$, where

$$F(c_j^n) = wc_{total} + (1-w)(c_j^n - R(\alpha(c_{total} - c_j^n), c_j^n)). \quad (24)$$

Next, we make use of the well-known result that one-dimensional maps that exhibit chaos must be nonmonotonic, i.e., must have at least one extremum (Ott, 1993). Thus, the presence of chaos in the present model implies that the map $c_j^{n+1} = F(c_j^n)$ should have this property, meaning that the derivative dF/dc_j^n should change sign over a range of c_j^n. It follows trivially from Eq. 24 that this condition is equivalent to

$$\frac{dR}{dc_j^n}\begin{cases} < 1 & c_j^n < c_j^* \\ > 1 & c_j^n > c_j^*, \end{cases} \quad (25)$$

where c_j^* corresponds to a local maximum of F. Therefore, if the total derivative dR/dc_j^n increases rapidly over some range of load, the above condition can be satisfied. To test whether this condition is satisfied directly from the ODEs of the model, we calculate $R \approx c_j^n - c_j^{n,min}$ versus c_j^n, where $c_j^{n,min}$ is the minimum SR concentration between times nT and $(n+1)T$. The result, which is shown in Fig. 10 *B*, shows that the slope of R changes from $dR/dc_j^n < 1$ to $dR/dc_j^n > 1$ over the range of SR loads explored by the chaotic trajectory. For the same trajectory, we also check that the conservation condition given by Eq. 21 holds, by plotting, in Fig. 10 *C*, c_i^n versus c_j^n. From the plot, we see that c_j^n is an approximately linear function of c_i^n, which confirms our assumption that c_i^n can be eliminated in favor of c_j^n using Eq. 21, and that the dynamical system can be reduced to a one-dimensional discrete map.

It is important to emphasize that the total derivative $dR/dc_j^n \equiv -\alpha\partial R/\partial c_i^n + \partial R/\partial c_j^n$ depends both on the steepness of the relations between release and load, and release and diastolic calcium, which is a consequence calcium-induced inactivation of I_{Ca}. Hence, the degree of nonlinearity of both relations contribute to the existence of a maximum in the map independent of the strength of the uptake current w. In contrast, the condition for instability ($dF/dc_j \geq 1$ or, equivalently, Eq. 23) depends on both the steepness of these relations and the strength of uptake. Finally, since the SR concentration is difficult to measure experimentally, we also plot, in Fig. 10 *D*, the peak cytosolic calcium concentration at one beat versus the next i.e., c_{peak}^{n+1} versus c_{peak}^n. Here, we find again a nonmonotonic relationship, which is a direct consequence of the condition given in Eq. 25.

Role of JSR-SR diffusional relaxation

In this section, we analyze in more detail the role of the JSR-SR relaxation time (τ_a) on the model behavior. Since there

are no experimental measurements of this quantity, we have evaluated the model properties for a wide range of relaxation times (1–100 ms). The primary effect of the relaxation time is to simply change the amount of calcium released from the SR. During release, the SR is drained by the current I_r that depends on the concentration of unrecruited JSR compartments (c_j'). However, the average concentration of unrecruited JSR compartments is higher than the average concentration in the SR, i.e., $c_j' > c_j$, since these JSR compartments have not been depleted, and are simply relaxing to the average concentration in the SR. Given that $Q(c_j')$ is a monotonically increasing function, then a longer delay time will allow more calcium to be drained from the SR since c_j' can remain large for a longer time. In Fig. 11, we plot the maximum change in total SR concentration for different initial SR loads (c_j^0), and for a relaxation time of 100 ms and 1 ms. It is clear that more calcium is released, for all initial JSR loads, when the relaxation time is large as opposed to when it is small.

Role of spark lifetime

In the remainder of this section, we explore in more detail the dependence of the nonlinearity responsible for calcium alternans on the physiological parameters of the model. In particular, we will focus on the role played by the spark lifetime (τ_r). Here, we will analyze the simplest case when I_{Ca} depends only on time, and where the relaxation time between c_j' and c_j is instantaneous. In this case the release from the SR is given by $R \approx c_j^0 - c_j^{min}$, where c_j^0 is the concentration before I_{Ca} is turned on, and where c_j^{min} is the minimum concentration in the SR. Also, since we have eliminated the calcium dependence of I_{Ca}, the condition for an unstable fixed point can be written as $R' = \partial R/\partial c_j > 1 + 1/(1 - w(T))$, where the partial derivative is evaluated at c_j^0. Since I_{Ca} peaks rapidly and decays in a time $\tau_m \sim 30$ ms, then most of the release occurs during the time τ_m. Thus, during the time interval τ_m after I_{Ca} is turned on we can write

$$\frac{dc_j(t)}{dt} \approx -I_r(t)$$

$$\frac{dI_r(t)}{dt} = gI_{Ca}(t)Q(c_j(t)) - I_r(t)/\tau_r, \tag{26}$$

where we have dropped the uptake current since it is small compared to $I_r(t)$. To explore the dependence of the load dependent nonlinearity on the spark lifetime, we study the behavior of R' for a range of τ_r while keeping $z = g\tau_r$ fixed. In Fig. 12 we plot the maximum slope R'_{max} versus τ_r for a range of z values. The important feature of the plots is that $R'_{max} \to 1$ as $\tau_r \to 0$, regardless of the value of z. Thus, in this case, a nonzero spark lifetime is essential to destabilize the periodic fixed point, which cannot occur if $R'_{max} < 2$. This result can be understood analytically by studying Eqs. 26 in the limit $\tau_r \to 0$. In this limit the dynamics of c_j is described by

$$\frac{dc_j(t)}{dt} = -zI_{Ca}(t)Q(c_j(t)), \tag{27}$$

which is exactly solvable for a given release function $Q(x)$. Furthermore, it can be shown that if $Q(x)$ is any monotonically increasing function, then $R'_{max} \leq 1$. This result suggests that constructing a model with a steep load dependence that can destabilize the periodic fixed point requires that the release flux at a given time depends on the SR concentration at earlier times. If the release flux depends only on the instantaneous SR concentration, then the periodic fixed point is always stable. Thus, in the model formulation, the finite spark lifetime plays an important role in the dynamical behavior of the model.

DISCUSSION

An important feature of the model is that the local release flux during a calcium spark is treated phenomenologically using an exponentially decaying time course, with a JSR load-dependent amplitude and a fixed decay time constant. The phenomenological model relies only on two essential

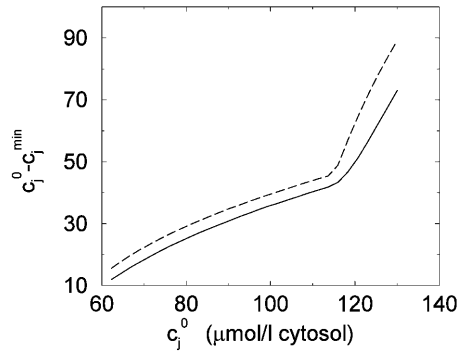

FIGURE 11 Dependence of the maximum change of total SR calcium concentration on the initial SR load. The dashed line corresponds to a JSR-SR relaxation time of $\tau_a = 100$ ms, and the solid line corresponds to $\tau_a = 1$ ms.

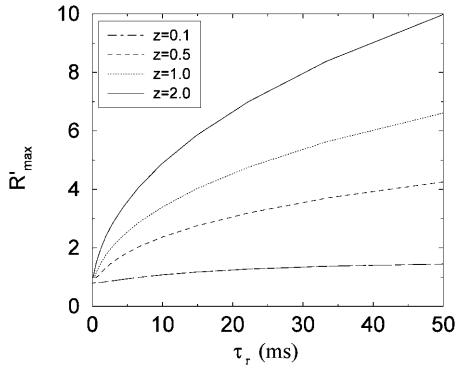

FIGURE 12 Plot of R'_{max} versus spark lifetime τ_r for different values of the parameter z.

properties of the local calcium dynamics. First, a strong dependence of the local release flux on the initial JSR concentration, and secondly, a finite lifetime of local release. The former is an immediate consequence of the regenerative nature of CICR, and the latter depends on the presence of a strong negative feedback mechanism that shuts off release. Thus, the model does not rely on a detailed spark termination mechanism, which still has not been established experimentally. An additional advantage of our approach is that we are able to incorporate into the model experimental measurements of the SR load dependence of release in the whole cell. This is a crucial input into the model, as the steep dependence of whole cell release on SR load has a profound impact on the dynamical behavior. Thus, the model construction takes into account both local properties of experimentally observed calcium sparks, and whole cell measurements of calcium release.

Another important property of the model is that it is able to reproduce the calcium alternans observed by Chudin et al. (1999), when it is paced by a clamped AP waveform that is fitted directly to that used in the experiment. At high pacing rates, calcium accumulates in the cell, and the corresponding increase in SR load and diastolic calcium levels promote a dynamical instability. Furthermore, by reducing the dynamics to a two-variable map, we have shown that the dynamical stability of the calcium system is determined by the functional dependence of the total release (R) on both the SR concentration and the diastolic concentration just before an AP upstroke. To our knowledge, only a steep dependence of total release on SR load has been considered previously as a possible mechanism for calcium transient alternans (Adler et al., 1985; Eisner et al., 2000). The present model shows that the dependence of release on diastolic calcium is also a possible destabilizing mechanism that can act in conjunction with or independently from the dependence of release on SR load. The physiological origin of the dependence of release on diastolic calcium is the calcium-induced inactivation of the L-type calcium current, i.e., a higher diastolic calcium leads to a reduced entry of calcium into the cell and hence to a smaller release.

The nonlinear dependence of release on SR load and diastolic calcium can be viewed as concentration-dependent restitution properties of the calcium system. This view point is analogous to that of electrical restitution, which gives a simplified description of the voltage dynamics by relating the diastolic interval at one beat to the APD at the next. In particular, the stability of the calcium system is determined by the quantity Γ, defined in Eq. 23, in much the same way that the stability of the voltage dynamics is determined by the slope of the electrical restitution curve.

At high pacing rates, and if the SR load dependence of release is made very steep, the calcium system can exhibit chaotic behavior under a periodic voltage clamp. This result can be understood by reducing the dynamics of calcium cycling to a one-dimensional discrete map that is non-monotonic, and hence can in principle exhibit chaos. In the past, chaotic dynamics has been observed in unclamped voltage measurements in ventricular tissue (Watanabe et al., 1995). In that case, the chaotic voltage dynamics was attributed to a biphasic (nonmonotonic) electrical restitution function. An alternate explanation is that since voltage is coupled to calcium, a chaotic dynamics of calcium cycling can lead to a corresponding chaotic behavior of voltage. Thus, even when the electrical restitution function is stable (slope <1) and monotonic, the coupling between voltage and calcium can lead to unstable voltage dynamics.

In the past, unstable voltage dynamics at the cellular level has been linked to arrhythmias at the level of the whole heart (Chialvo et al., 1990; Garfinkel et al., 1992). Thus, calcium cycling, by having a destabilizing effect on voltage, may promote arrhythmias in the heart. To address this possibility, it is crucial to understand the bidirectional coupling between voltage and calcium under unclamped conditions at a wide range of pacing rates. Moreover, it is crucial to investigate not only the dynamics at the cellular scale but also at the tissue scale. The computational tractability of the phenomenological model presented here should serve as a useful computational tool to begin to address these problems. More detailed mechanistic models of calcium cycling, which attempt to model calcium dynamics at the dyadic junction level, are still far too computationally costly to be useful in this regard. For instance, the most recent computational model of Greenstein and Winslow (2002), requires a run time of $\sim$40 min on 10 parallel SGI Power Challenge R10,000 processors to simulate a whole cell calcium transient over a 1 s interval. On the other hand, the model ODEs presented here require $\sim$0.1 s of run time on a single Compaq Alpha EV6.7 667MHz processor, for a simulation over the same time interval. This computational speedup of roughly five orders of magnitude is crucial to begin to investigate, via numerical simulation, the possible link between abnormalities in calcium cycling at the cellular scale and arrhythmias in the whole heart.

The steep load dependence of release, which plays a crucial role in the dynamical instability, is consistent with the experimental work of Bassani et al. (1995). There are several possible reasons why release should increase steeply with SR load at high loads. One interesting possibility is that increasing the SR load may induce regenerative release between neighboring dyads. In other words, at high load, a ''spark'' may be due to clusters of dyads (macrosparks), rather than a single dyad. As the SR load is increased further, these clusters will grow, and the amount released may increase rapidly with small changes in SR load. This hypothesis is supported by the fact that increasing SR load even slightly more than $c_j \sim 100$ μmol/l cytosol leads to spontaneous release (Bassani et al., 1995). Thus, the CICR induced cooperativity between neighboring dyads may underlie the nonlinear behavior of release at the whole cell level. To clarify further, it should be noted that this nonlinear

load dependence does not describe an arbitrarily defined spontaneous release process, but rather, reflects an inherent instability of the release mechanism.

An important question to consider is whether the JSR-SR relaxation time can be the primary mechanism that underlies calcium alternans at high pacing rates. Based on the available experimental data on calcium alternans, we will argue that this is unlikely to be the case. First, calcium alternans, when induced under rapid pacing, typically occur around cycle lengths of 200 ms. However, the relaxation time between c_j' and c_j is at most 100 ms, and so there is more than enough time for the JSR to relax to the SR concentration at the rates when calcium alternans are observed. An even stronger argument can be made by noting that alternans can be induced at normal pacing rates ($T \sim 1$ s) by application of various external agents such as tetracaine (Diaz et al., 2002). These external agents are known to have a direct effect on the RyR channels, and are unlikely to change the mobility of calcium inside the SR. Moreover, we find in our model simulations that over a wide range of relaxation times (τ_a), the dynamics of the calcium system does not exhibit alternans at high rates unless a steep load dependence and calcium-induced inactivation is invoked. These findings suggest that the mechanism that underlies alternans is crucially dependent on the RyR release mechanism rather than the JSR-SR relaxation time.

Another possible physiological mechanism that may underlie alternans is nonlinear buffering. The mathematical analysis presented in the section ''Map reduction with linear instantaneous buffering'' assumed for simplicity linear buffering. Therefore, this analysis does not address the dynamical role of nonlinear buffering. In our model simulations, we find that nonlinear buffering in the cytosol cannot induce alternans without a corresponding steep dependence of release on SR load or on diastolic calcium. However, the onset and amplitude of alternans does depend on the nonlinear buffering kinetics. These results suggest that, with realistic experimentally derived parameters, nonlinear buffering influences, but is not solely responsible for, calcium alternans.

The rise in calcium at high rates depends primarily on the corresponding accumulation of sodium, due to the activity of the NaCa exchange current (Harrison and Boyett, 1995). As the sodium concentration in the cell rises, the Nernst equilibrium potential of the exchange current is shifted such that calcium influx is favored. Another mechanism that promotes calcium loading at high rates is that the AP waveform spends more time per period at plateau potentials, and so the time spent in the calcium efflux mode is reduced. However, we found in our simulations that this effect alone, keeping intracellular sodium fixed, is not enough to account for the large increase of c_i^{max} at high rates. Thus, our results suggest that sodium accumulation is essential for calcium loading at high rates, and is probably what underlies the positive force frequency relation that is observed in ventricular myocytes.

CONCLUSIONS

In summary, we have presented a physiologically motivated model of calcium cycling under AP clamp conditions. A key feature of this model is to represent the release of calcium from the SR as a sum of spatially localized events that correspond to calcium sparks. The rate at which sparks are recruited is assumed to be directly proportional to the whole cell L-type calcium current (I_{Ca}). This assumption is consistent with experiments of simultaneous measurements of spark occurrence and whole cell I_{Ca} (Collier et al., 1999). Moreover, this choice naturally yields graded release, consistent with Stern's local control hypothesis (Stern, 1992). An important advantage of this model is that it incorporates known constitutive relationships between experimentally measurable quantities such as fractional release and SR load. Furthermore, it is computationally tractable, and can be used to explore the dynamical behavior of the calcium system under a wide range of pacing rates. At high rates, the model is able to reproduce sustained calcium alternans, consistent with experimental observations (Chudin et al., 1999).

By reducing the dynamics to a two-variable map of the concentrations from one beat to the next, we were able to analyze the nonlinear dynamics of the calcium system in more detail. This analysis revealed that the dynamical instability that underlies calcium alternans is due to the functional dependence of release on both the SR load and the diastolic calcium concentration. We also find that under plausible physiological conditions, the calcium system can exhibit chaos when it is driven by a periodic AP clamp. By further simplifying the discrete map to one variable, we show that the chaotic dynamics can be traced to a nonmonotonic functional relationship between the peak calcium concentration at one beat versus that at the previous beat.

Furthermore, we found that the degree of nonlinearity is sensitive to physiologically measurable quantities such as the spark lifetime and the strength of the uptake current. Hence, the model not only sheds light on the dynamical behavior of the calcium system, but also gives insight on how physiological properties of the calcium cycling machinery influence the dynamics. An interesting future prospect is to pace this model under unclamped conditions to explore the full range of dynamical behavior of the coupled voltage and calcium systems.

APPENDIX A: MODEL OF LOCAL DYNAMICS

In this appendix, we describe a simplified model of calcium dynamics within the dyadic junction. The goal here is to test the assumptions behind our phenomenological description of local calcium release during a spark (Eq. 4), using a plausible model of the local calcium dynamics. The relevant dynamical variables are the free concentration in the local dyadic space c_p, and the free concentration c_{jsr}^f of the local JSR. Here, we have dropped the superscript k, since there is no need to distinguish between different dyadic junctions. We will assume constant linear buffering so that $c_p^{total} = B_p c_p$ and $c_{jsr} = B_{jsr} c_{jsr}^f$, where B_p and B_{jsr} are constants. Here, B_{jsr} will be chosen

so that the free JSR concentration before release will be in the range 500–1500 μM.

The free concentrations obey the ODEs

$$\frac{dc_p}{dt} = \alpha(I_{rel} - I_d + i_{Ca})$$

$$\frac{dc_{jsr}^f}{dt} = -I_{rel} + I_{tr}, \tag{28}$$

where I_{rel} is the flux of calcium from the JSR, I_d is the diffusion of calcium into the submembrane space, i_{Ca} is the current from the local L-type channels, and I_{tr} is the diffusion of calcium from the NSR into the JSR. Here, $\alpha = B_{jsr}\upsilon_{jsr}/B_p\upsilon_p$, where υ_p and υ_{jsr} are the volumes of the dyadic space and JSR, respectively. The release current is given by $I_{rel} = g_s a(c_{jsr}^f - c_p)$, with g_s a constant that denotes the maximum conductance of the RyR cluster, and where a is the open probability. To simulate CICR, the states of the RyR cluster are modeled using a simple reaction scheme, where the transition rate from closed to open states is proportional to the square of c_p. This yields $da/dt = (a_\infty - a)/\tau_a$, with $a_\infty = c_p^2/(c_p^2 + c_p^{*2})$ and $\tau_a = 1/(k_d(c_p^2 + c_p^{*2}))$, where k_d is the deactivation rate. The threshold for regenerative release is determined by the concentration c_p^*. Given the small volume of the dyadic space, a brief opening of the L-type channels is sufficient to raise c_p to levels much higher than in the myoplasm. Thus, to ensure that regenerative release can only be initiated by the local L-type channels, and not by a rise of calcium in the submembrane space, it is crucial that the threshold $c_p^*$is larger than the peak concentration in the submembrane space ($\sim$10 μM). Thus, in this model we will use a high threshold $c_p^* = 65$ μM, which is further supported by the fact that, under normal conditions, release from a dyadic junction typically does not trigger release from neighboring junctions.

The diffusion of calcium away from the dyadic space is modeled using $I_d = (c_p - c_s)/\tau_p$, where τ_p is chosen so that c_p relaxes to c_s in 0.05 ms, which is roughly the same as the time for a calcium ion to diffuse across the 100 nm dyadic cleft. Also, we model diffusion between the NSR and JSR with $I_{tr} = (c_{nsr}^f - c_{jsr}^f)/\tau_{tr}$, where c_{nsr}^f is the free concentration of the bulk NSR, and where τ_{tr} is chosen so that c_{jsr}^f relaxes to c_{nsr}^f in $\sim$50 ms. To simulate a spark, we will solve Eqs. 28 with c_s and c_{nsr}^f held constant. The initial concentrations in the dyadic space and the JSR are denoted by c_p^0 and c_{jsr}^0, respectively, with $c_p^0 = c_s$ and $c_{jsr}^0 = c_{nsr}$. A spark is initiated by the trigger current, which will be a square pulse of 4 ms duration and amplitude 0.05 pA. All parameters of the model are listed in Table 6.

During a simulated spark, c_p rises rapidly to $\sim$200 μM within several milliseconds, and then decays over the next 10–30 ms. The initial rise in c_p is due to the positive feedback of CICR, during which the open probability of the RyR rises, and $I_{rel} \gg I_d$. However, this lasts only for a short time since I_{rel} rapidly decreases as c_p approaches c_{jsr}^f, and I_d increases as c_p grows much larger than c_s. Since the JSR is being replenished in a timescale that is slower than the diffusion away from the dyadic space, then within a few milliseconds we have $I_d > I_{rel}$, in which case c_p begins to decline. Since the threshold for activation c_p^* is high, the release flux is robustly terminated as c_p drops bellow c_p^*. Thus, in this local model, calcium diffusion away from the dyadic space, in concert with JSR depletion and a high a threshold for local CICR, yields a robust spark termination mechanism.

In Fig. 13 *A*, we plot the current flux from a JSR during a spark as a function of time for different initial JSR loads. From the graph, we can see that the duration of the release flux increases from 10 to 30 ms as the total initial JSR concentration is increased from 70 to 150 μM. In Fig. 13 *B*, we plot the maximum release current during a spark as a function of the dyadic space concentration before CICR is initiated (c_p^0). It is clear from the plot that the peak flux from the SR remains fairly constant as a function of c_p^0. On the other hand, as seen in Fig. 13 *C*, if we vary the initial JSR load (c_{jsr}^0), the peak release current changes substantially. These results corroborate our initial assumption that the local release flux during a spark can be well approximated by a strong JSR load dependence, and an effectively constant spark lifetime.

TABLE 5 Cytosolic Buffering parameters

Parameter	Definition	Value
B_T	Total concentration of troponin C	70 μmol/l cytosol
B_{SR}	Total concentration of SR binding sites	47 μmol/l cytosol
B_{Cd}	Total concentration of calmodulin binding sites	24 μmol/l cytosol
k_{on}^T	On rate for troponin C	32.7/μMs
k_{off}^T	Off rate for troponin C	19.6/s
K_{SR}	Dissociation constant for SR binding sites	0.6 μM
K_{Cd}	Dissociation constant for calmodulin binding sites	7 μM

TABLE 6 Parameters for local dynamics

Parameter	Definition	Value
g_s	Maximum RyR cluster conductance	120 s^{-1}
c_p^*	RyR activation threshold	65 μM
τ_p	Diffusion flux time constant	0.0025 s
τ_{tr}	JSR refilling time constant	0.05 s
υ_{jsr}	JSR volume	10^{-6} υ_i
k_d	RyR deactivation rate	0.5 s^{-1} (μM)$^{-2}$
α	Buffer and volume ratio	50

APPENDIX B: IONIC CURRENTS

L-type calcium current

We model the L-type calcium current (I_{Ca}) based on the most recent experimental measurements in rabbit myocytes at a temperature of 35°C (see Fig. 7 *D* in Puglisi et al. (1999)). The voltage gates are modeled using

$$d_\infty(V) = \frac{1}{1 + \exp[-(V-5)/6.24]},$$

$$f_\infty(V) = \frac{1}{1 + \exp[(V+35)/8.6]}. \tag{29}$$

We have taken the d gate to be instantaneous since τ_d is the fastest timescale in the model (<5 ms), given that fast sodium currents are not incorporated in the model. We will take the relaxation time of the f gate to be a constant τ_f in the range 30–50 ms. This is different from the standard formulation in Luo-Rudy II, where τ_f is taken to have a U-shaped dependence on voltage. However, given that the inactivation properties of the L-type current are both voltage and calcium dependent, it is difficult to measure a purely voltage-dependent quantity such as τ_f. For a more extensive discussion on this point, see the experimental article of Linz and Meyer (1998). Moreover, we found that we could not reproduce the experimental measurements of Puglisi et al. (1999) using the standard formulation of τ_f.

To model calcium-induced inactivation, we use $\tilde{c}_s = 0.5$ μM, and adjust k_o so that τ_q is in the 10–50 ms range, since experiments (Linz and Meyer (1998); Puglisi et al. (1999)) have shown that calcium-induced inactivation is typically faster than voltage inactivation. The single-channel L-type current is the same as in Luo-Rudy II, and is given by

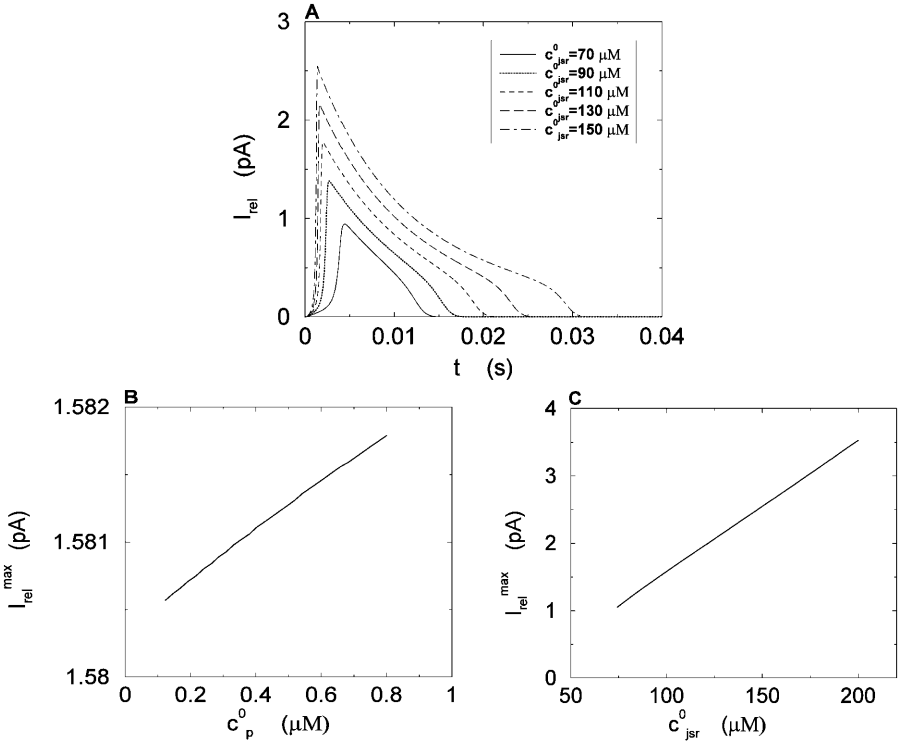

FIGURE 13 Local release flux I_{rel} during a calcium spark. (*A*) Plot of I_{rel} versus t for various JSR loads. The initial concentration within the dyadic space is $c_p^0 = 0.1\ \mu$M for all cases. (*B*) Plot of the maximum release current I_{rel}^{max} for different initial dyadic concentrations c_p^0. The initial total JSR concentration c_{jsr}^0 is fixed at 100 μM. (*C*) Plot of I_{rel}^{max} for different initial JSR loads. For all points $c_p^0 = 0.1\ \mu$M.

$$Mi_{Ca} = \bar{i}_{Ca} P_{Ca} \frac{4VF^2}{RT} \left(\frac{c_s \exp(2a) - 0.341\, Ca_o}{\exp(2a) - 1} \right), \qquad (30)$$

where $\bar{i}_{Ca}$ is an adjustable constant. Note that the number of dyadic junctions M, which is constant, is absorbed into $\bar{i}_{Ca}$. Here, $Ca_o = [Ca^{2+}]_o$ corresponds to the external calcium concentration, and $a = VF/RT$.

NaCa exchange current

The sodium calcium exchange current as formulated in Luo-Rudy II is given by

$$I_{NaCa} = \bar{I}_{NaCa} \frac{1}{K_{m,Na}^3 + Na_o^3} \cdot \frac{1}{K_{m,Ca} + Ca_o} \times \frac{e^{\xi a} Na_i^3 Ca_o - e^{(\xi-1)a} Na_o^3 c_s}{1 + k_{sat} e^{(\xi-1)a}}, \qquad (31)$$

where the external sodium concentration is $Na_o = [Na^+]_o$. Also, $\bar{I}_{NaCa}$ is an adjustable constant that will be used to adjust the strength of the exchanger.

Uptake current

The uptake current is taken to have the simple form

$$I_{up}(c_i) = \frac{v_{up} c_i^2}{c_i^2 + c_{up}^2}. \qquad (32)$$

The parameters used in the model are given in Tables 1–4.

APPENDIX C: CYTOSOLIC CALCIUM BUFFERING

The amount of calcium in the bulk myoplasm that is bound to troponin C will be denoted by $[CaT]_i$, and satisfies

$$\frac{d[CaT]_i}{dt} = I_{trpn}^i, \qquad (33)$$

where $I_{trpn}^i = k_{on}^T\, c_i (B_T - [CaT]_i) - k_{off}^T [CaT]_i$. The on and off rate constants and the total concentration of troponin C (B_T) have been reported previously (Shannon et al., 2000a), and are listed in Table 5. The buffering to SR membrane and calmodulin binding sites are approximated using the rapid buffering approximation (Wagner and Keizer, 1994). This effect is taken into account using

$$\beta(c_i) = \left[1 + \frac{B_{SR} K_{SR}}{(c_i + K_{SR})^2} + \frac{B_{Cd} K_{Cd}}{(c_i + K_{Cd})^2} \right]^{-1}, \qquad (34)$$

where K_{SR} and K_{Cd} are the buffer dissociation constants for the SR and calmodulin buffers, respectively, and where B_{SR} and B_{Cd} denote the total concentration of the respective buffers. The values of these parameters are known experimentally (Shannon et al., 2000a) and are listed in Table 5. Note that for buffering in the submembrane space, we simply replace c_i with c_s, and $[CaT]_i$ with $[CaT]_s$.

The authors acknowledge Professor Godfrey L. Smith, Glasgow University, for reading the manuscript and providing helpful comments. We also thank the referees for several helpful suggestions.

This research was supported in part by National Institutes of Health Special Centers of Research in Sudden Cardiac Death P50-HL52319, and by the Kawata and Laubisch endowments.

REFERENCES

Adler, D., A. Y. K. Wong, and Y. Mahler. 1985. Model of mechanical alternans in the mammalian myocardium. *J. Theor. Biol.* 117:563–577.

Bassani, J. W. M., W. Yuan, and D. M. Bers. 1995. Fractional SR Ca release is regulated by trigger Ca and SR Ca content in cardiac myocytes. *Am. J. Physiol. Cell Physiol.* 268:C1313–C1319.

Bers, D. M. 2001. Excitation-Contraction Coupling and Cardiac Contractile Force. Kluwer, Boston.

Cannell, M. B., H. Cheng, and W. J. Lederer. 1994. Spatial non-uniformities in $[Ca^{2+}]_i$ during excitation-contraction coupling in cardiac myocytes. *Biophys. J.* 67:1942–1956.

Cannell, M. B., and C. Soeller. 1997. Numerical analysis of ryanodine receptor activation by L-type channel activity in the cardiac muscle dyad. *Biophys. J.* 73:112–122.

Cheng, H., W. J. Lederer, and M. B. Cannell. 1993. Calcium sparks: elementary events underlying excitation-contraction coupling in heart muscle. *Science.* 262:740–744.

Chialvo, D. R., R. F. Gilmour, Jr., and J. Jalife. 1990. Low dimensional chaos in cardiac tissue. *Nature.* 343:653–657.

Chudin, E., J. Goldhaber, A. Garfinkel, J. Weiss, and B. Kogan. 1999. Intracellular Ca^{2+} dynamics and the stability of ventricular tachycardia. *Biophys. J.* 77:2930–2941.

Cleemann, L., W. Wang, and M. Morad. 1998. Two-dimensional confocal images of organization, density, and gating of focal Ca^{2+} release sites in rat cardiac myocytes. *Proc. Natl. Acad. Sci. USA.* 95:10984–10989.

Collier, M. L., A. P. Thomas, and J. R. Berlin. 1999. Relationship between L-type Ca^{2+} current and unitary sarcoplasmic reticulum Ca^{2+} release events in rat ventricular myocytes. *J. Physiol.* 516:117–128.

DelPrincipe, F., M. Egger, and E. Niggli. 1999. Calcium signalling in cardiac muscle: refractoriness revealed by coherent activation. *Nat. Cell Biol.* 1:323–329.

Diaz, M. E., D. A. Eisner, and S. C. O'Neill. 2002. Depressed ryanodine receptor activity increases variability and duration of the systolic Ca^{2+} transient in rat ventricular myocytes. *Circ. Res.* 91:585–593.

Eisner, D. A., H. S. Choi, M. E. Diaz, S. C. O'Neill, and A. W. Trafford. 2000. Integrative analysis of calcium cycling in cardiac muscle. *Circ. Res.* 87:1087–1094.

Faber, G. M., and Y. Rudy. 2000. Action potential and contractility changes in $[Na^+]_i$ overloaded cardiac myocytes: a simulation study. *Biophys. J.* 78:2392–2404.

Fabiato, A. 1983. Calcium-induced release of calcium from the cardiac sarcoplasmic reticulum. *Am. J. Physiol.* 245:C1–14.

Fox, J. F., J. L. McHarg, and R. F. Gilmour. 2002. Ionic mechanisms of electrical alternans. *Am. J. Physiol. Heart Circ. Physiol.* 282: H516–H530.

Forbes, M. S., L. A. Hawkey, S. K. Jirge, and N. Sperelakis. 1985. The sarcoplasmic reticulum of mouse heart: its divisions, configurations, and distribution. *J. Ultrastruct. Res.* 93:1–16.

Franzini-Armstrong, C., F. Protasi, and V. Ramesh. 1999. Shape, size, and distribution of Ca^{2+} release units and couplons in skeletal and cardiac muscles. *Biophys. J.* 77:1528–1539.

Garfinkel, A., M. L. Spano, W. L. Ditto, and J. N. Weiss. 1992. Controlling cardiac chaos. *Science.* 257:1230–1235.

Glukhovsky, A., D. R. Adam, G. Amitzur, and S. Sideman. 1998. Mechanism of Ca^{2+} release from the sarcoplasmic reticulum: a computer model. *Ann. Biomed. Eng.* 26:213–229.

Greenstein, J. L., and R. L. Winslow. 2002. An integrative model of the cardiac ventricular myocyte incorporating local control of Ca^{2+} release. *Biophys. J.* 83:2918–2945.

Harrison, S. M., and M. R. Boyett. 1995. The role of the Na^+-Ca^{2+} exchanger in the rate-dependent increase in contraction in guinea-pig ventricular myocytes. *J. Physiol.* 482:555–566.

Hund, T. J., N. F. Otani, and Y. Rudy. 2000. Dynamics of action potential head-tail interaction during reentry in cardiac tissue: ionic mechanisms. *Am. J. Physiol. Heart Circ. Physiol.* 279:H1869–H1879.

Jafri, S., J. J. Rice, and R. L. Winslow. 1998. Cardiac Ca^{2+} dynamics: the roles of ryanodine receptor adaptation and sarcoplasmic reticulum load. *Biophys. J.* 74:1149–1168.

Linz, K. W., and R. Meyer. 1998. Control of L-type current during the action potential of guinea pig ventricular myocytes. *J. Physiol.* 513: 425–442.

Lopez-Lopez, J. R., P. S. Shacklock, C. W. Balke, and W. G. Wier. 1995. Local calcium transients triggered by single L-type calcium channel currents in cardiac cells. *Science.* 268:1042–1045.

Lukyanenko, V., I. Gyorke, and S. Gyorke. 1996. Regulation of calcium release by calcium inside the sarcoplasmic reticulum in ventricular myocytes. *Pflugers Arch.* 432:1047–1054.

Lukyanenko, V., S. Viatchenko-Karpinski, A. Smirnov, T. F. Weisner, and S. Gyorke. 2001. Dynamic regulation of sarcoplasmic reticulum Ca^{2+} content and release by luminal Ca^{2+}-sensitive leak in rat ventricular myocytes. *Biophys. J.* 81:785–798.

Luo, C. H., and Y. Rudy. 1994. A dynamic model of the cardiac ventricular action potential. I. Simulations of ionic currents and concentration changes. *Circ. Res.* 74:1071–1096.

Meissner, G. 1994. Ryanodine receptor/Ca^{2+} release channels and their regulation by endogenous effectors. *Annu. Rev. Physiol.* 56:485–508.

Niggli, E. 1999. Localized intracellular calcium signaling in muscle: calcium sparks and calcium quarks. *Annu. Rev. Physiol.* 61:311–335.

Nolasco, J. B., and R. W. Dahlen. 1968. A graphic method for the study of alternation in cardiac action potential. *J. Appl. Physiol.* 25:191–196.

Ott, E. 1993. Chaos in Dynamical Systems. Cambridge University Press, New York.

Peskoff, A., and G. A. Langer. 1998. Calcium concentration and movement in the ventricular cardiac cell during an excitation-contraction cycle. *Biophys. J.* 74:153–174.

Puglisi, J. L., W. Yuan, J. W. M. Bassani, and D. M. Bers. 1999. Ca^{2+} influx through Ca^{2+} channels in rabbit ventricular myocytes during action potential clamp: influence of temperature. *Circ. Res.* 85:e7–e16.

Rice, J. J., M. S. Jafri, and R. L. Winslow. 1999. Modeling gain and gradedness of Ca^{2+} release in the functional unit of the cardiac diadic space. *Biophys. J.* 77:1871–1884.

Sah, R., R. J. Ramirez, and P. H. Backx. 2002. Modulation of Ca^{2+} release in cardiac myocytes by changes in repolarization rate: role of phase-1 action potential repolarization in excitation-contraction coupling. *Circ. Res.* 90:165–173.

Shannon, T. R., K. S. Ginsburg, and D. M. Bers. 2000a. Reverse mode of the sarcoplasmic reticulum calcium pump and load-dependent cytosolic calcium decline in voltage-clamped cardiac myocytes. *Biophys. J.* 78: 322–333.

Shannon, T. R., K. S. Ginsburg, and D. M. Bers. 2000b. Potentiation of fractional sarcoplasmic reticulum calcium release by total and free intra-sarcoplasmic reticulum calcium concentration. *Biophys. J.* 78:334–343.

Snyder, S. M., B. M. Palmer, and R. L. Moore. 2000. A mathematical model of cardiocyte Ca^{2+} dynamics with a novel representation of sarcoplasmic reticular Ca^{2+} control. *Biophys. J.* 79:94–115.

Sobie, E. A., K. W. Dilly, J. S. Cruz, W. J. Lederer, and M. S. Jafri. 2002. Termination of cardiac Ca^{2+} sparks: an investigative mathematical model of calcium-induced calcium release. *Biophys. J.* 83:59–78.

Soeller, C., and M. B. Cannell. 1999. Examination of the transverse tubular system in living cardiac rat myocytes by 2-photon microscopy and digital image-processing techniques. *Circ. Res.* 84:266–275.

Stern, M. D. 1992. Theory of excitation-contraction coupling in cardiac muscle. *Biophys. J.* 63:497–517.

Stern, M. D., L. S. Song, H. Cheng, J. S. Sham, H. T. Yang, K. R. Boheler, and E. Rios. 1999. Local control models of cardiac excitation-contraction coupling. A possible role of allosteric interactions between ryanodine receptors. *J. Gen. Physiol.* 113:469–489.

Viswanathan, P. C., R. M. Shaw, and Y. Rudy. 1999. Effects of I_{Kr} and I_{Ks} heterogeneity on action potential duration and its rate dependence. *Circulation*. 99:2466–2474.

Wagner, J., and J. Keizer. 1994. Effects of rapid buffers on Ca^{2+} diffusion and Ca^{2+} oscillations. *Biophys. J.* 67:447–456.

Wang, S., L. Song, E. G. Lakatta, and H. Cheng. 2001. Ca^{2+} signalling between single L-type Ca^{2+} channels and ryanodine receptors in heart cells. *Nature*. 410:592–596.

Watanabe, M., N. F. Otani, and R. F. Gilmour, Jr. 1995. Biphasic restitution of action potential duration and complex dynamics in ventricular myocardium. *Circ. Res.* 76:915–921.

Weber, C. R., V. Piacentino, III, K. S. Ginsburg, S. R. Houser, and D. M. Bers. 2001. Na^{+}-Ca^{2+} exchange current and submembrane [Ca^{2+}] during the cardiac action potential. *Circ. Res.* 90:182–189.

Wier, W. G., and C. W. Balke. 1999. Ca^{2+} release mechanisms, Ca^{2+} sparks, and local control of excitation-contraction coupling in normal heart muscle. *Circ. Res.* 85:770–776.

Wier, W. G., T. M. Egan, J. R. Lopez-Lopez, and C. W. Balke. 1994. Local control of excitation-contraction coupling in rat heart cells. *J. Physiol.* 474:463–471.